2009

LARGE AREA SURVEY FOR z=7 GALAXIES IN SDF AND GOODS-N: IMPLICATIONS FOR GALAXY FORMATION AND COSMIC REIONIZATION

M Ouchi

B Mobasher

K Shimasaku

HC Ferguson

SM Fall

See next page for additional authors

Recommended Citation

Ouchi, M; Mobasher, B; Shimasaku, K; Ferguson, HC; Fall, SM; Ono, Y; Kashikawa, N; Morokuma, T; Nakajima, K; Okamura, S; Dickinson, M; Giavalisco, M; and Ohta, K, "LARGE AREA SURVEY FOR z=7 GALAXIES IN SDF AND GOODS-N: IMPLICATIONS FOR GALAXY FORMATION AND COSMIC REIONIZATION" (2009). *Astrophysical Journal*. 160.
https://doi.org/https://doi.org/10.1088/0004-637X/706/2/1136

The Astrophysical Journal, 706:1136–1151, 2009 December 1 doi:10.1088/0004-637X/706/2/1136

LARGE AREA SURVEY FOR $z = 7$ GALAXIES IN SDF AND GOODS-N: IMPLICATIONS FOR GALAXY FORMATION AND COSMIC REIONIZATION*

Masami Ouchi[1,11], Bahram Mobasher[2], Kazuhiro Shimasaku[3,4], Henry C. Ferguson[5,6], S. Michael Fall[5], Yoshiaki Ono[3], Nobunari Kashikawa[7], Tomoki Morokuma[7,12], Kimihiko Nakajima[3], Sadanori Okamura[3,4], Mark Dickinson[8], Mauro Giavalisco[9], and Kouji Ohta[10]

[1] Observatories of the Carnegie Institution of Washington, 813 Santa Barbara Street, Pasadena, CA 91101, USA; ouchi@obs.carnegiescience.edu
[2] Department of Physics and Astronomy, University of California, Riverside, CA 92521, USA
[3] Department of Astronomy, School of Science, University of Tokyo, Tokyo 113-0033, Japan
[4] Research Center for the Early Universe, School of Science, University of Tokyo, Tokyo 113-0033, Japan
[5] Space Telescope Science Institute, 3700 San Martin Drive, Baltimore, MD 21218, USA
[6] Department of Physics and Astronomy, Johns Hopkins University, 3400 N. Charles Street, Baltimore, MD 21218, USA
[7] Optical and Infrared Astronomy Division, National Astronomical Observatory, Mitaka, Tokyo 181-8588, Japan
[8] NOAO, 950 N. Cherry Avenue, Tucson, AZ 85719, USA
[9] Department of Astronomy, University of Massachusetts, Amherst, MA 01003, USA
[10] Department of Astronomy, Kyoto University, Kyoto 606-8502, Japan
Received 2009 August 22; accepted 2009 October 13; published 2009 November 10

ABSTRACT

We present results of our large area survey for z'-band dropout galaxies at $z = 7$ in a 1568 arcmin^2 sky area covering the SDF and GOODS-N fields. Combining our ultra-deep *Subaru*/Suprime-Cam z'- and y-band ($\lambda_{\rm eff} = 1\ \mu$m) images with legacy data of *Subaru* and *Hubble Space Telescope*, we have identified 22 bright z-dropout galaxies down to $y = 26$, one of which has a spectroscopic redshift of $z = 6.96$ determined from Lyα emission. The $z = 7$ luminosity function yields the best-fit Schechter parameters of $\phi^* = 0.69^{+2.62}_{-0.55} \times 10^{-3}$ Mpc^{-3}, $M^*_{\rm UV} = -20.10 \pm 0.76$ mag, and $\alpha = -1.72 \pm 0.65$, and indicates a decrease from $z = 6$ at a $> 95\%$ confidence level. This decrease is beyond the cosmic variance in our two fields, which is estimated to be a factor of $\lesssim$2. We have found that the cosmic star formation rate density drops from the peak at $z = 2$–3 to $z = 7$ roughly by a factor of $\sim$10 but not larger than $\sim$100. A comparison with the reionization models suggests either that the universe could not be totally ionized by only galaxies at $z = 7$, or more likely that properties of galaxies at $z = 7$ are different from those at low redshifts having, e.g., a larger escape fraction ($\gtrsim$0.2), a lower metallicity, and/or a flatter initial mass function. Our SDF z-dropout galaxies appear to form 60 Mpc long filamentary structures, and the $z = 6.96$ galaxy with Lyα emission is located at the center of an overdense region consisting of four UV bright dropout candidates, which might suggest an existence of a well-developed ionized bubble at $z = 7$.

Key words: cosmology: observations – galaxies: formation – galaxies: high-redshift

1. INTRODUCTION

Recent results from deep galaxy surveys have raised exciting questions about cosmic reionization and the early phases of galaxy formation. These surveys have extended the redshift frontier to $z \sim$ 6–10, using various techniques (Iye et al. 2006; Stark et al. 2007; Ota et al. 2008; Richard et al. 2008; Ouchi et al. 2009; Bouwens et al. 2008, 2009a, 2009b; Oesch et al. 2009a, 2009b; Castellano et al. 2009; McLure et al. 2009a, 2009b; Bunker et al. 2009; Hickey et al. 2009; Henry et al. 2007, 2008, 2009; Bradley et al. 2008; Zheng et al. 2009; Sobral et al. 2009). These observations have reached near the epoch of reionization at $z > 6$, which is suggested by Fan et al. (2006), who find that the Gunn–Peterson (GP) optical depths of SDSS QSOs significantly increase at $z \sim 6$. Although this increase can be explained by the extrapolation from low z to $z > 6$ via adoption of lognormal distribution for optical depths (Becker et al. 2007), it is also true that GP optical depths appear to increase significantly at around $z = 6$. The ionizing sources at $z \simeq 6$ are efficiently identified by i'-dropout technique (Stiavelli et al. 2004; cf. Bunker et al. 2004). However, the relation between reionization and ionizing sources, i.e., galaxies, are still not clear in our understanding of cosmic reionization. Since the WMAP5 polarization data indicate possible scenarios of an instantaneous reionization at $z = 11 \pm 1.4$ and an extended reionization at $z \sim$ 6–11 (Dunkley et al. 2009), the ionizing photon production rate of galaxies at this epoch would constrain these models of reionization history. It is suggested that a substantial fraction of galaxies have completed their starburst phase before $z \simeq 6$. Eyles et al. (2007) have shown that about 40% of the IRAC detected $z \simeq 6$ dropout galaxies exhibit a significant Balmer break, indicating that these are post-starburst galaxies whose major formation phase ended at $z > 6$.[13] It is important to understand when and how the progenitors of these post-starburst galaxies were formed. To address these questions, we need to study $z \gtrsim 7$ galaxies over a wide range of magnitudes to derive UV luminosity function (LF) and density.

Currently, only a handful of $z \simeq 7$ dropout galaxy candidates are photometrically identified, due to observational difficulties of identifying $z \simeq 7$ dropout galaxies whose detectable continuum is redshifted to 1 μm (e.g., Bouwens et al. 2008; Oesch

* Based on data obtained with the *Subaru Telescope*, the NASA/ESA *Hubble Space Telescope* (*HST*), and *Spitzer Space Telescope*. The *Subaru Telescope* is operated by the National Astronomical Observatory of Japan. *HST* is operated by the Association of Universities for Research in Astronomy (AURA), Inc., under NASA contract NAS5-26555. The *Spitzer Space Telescope* is operated by the Jet Propulsion Laboratory, California Institute of Technology under a contract with NASA.
[11] Carnegie Fellow
[12] Research Fellow of the Japan Society for the Promotion of Science
[13] Recently, Schaerer & de Barros (2009) argue that Eyles et al. (2007) would overestimate the Balmer breaks by the contributions of nebular emission to their broadband photometry.

et al. 2009a). Although *Hubble Space Telescope* (*HST*) images can reach as deep as ∼29 AB magnitude in near-infrared (NIR) bands with the state-of-the-art Wide-Field Camera 3 (WFC3), the number of $z \simeq 7$ dropout galaxy candidates is still limited up to ≃10–20, so far (Oesch et al. 2009b; McLure et al. 2009b; Bunker et al. 2009; also see Bouwens et al. 2009b). Moreover, the present studies cover only small areas (≃5 arcmin^2 for the *HST*/WFC3 studies and ≃100 arcmin^2 even for recent VLT/HAWK-I observations; Castellano et al. 2009; Hickey et al. 2009) or small volumes by the gravitational lensing technique (e.g., ∼100 Mpc^3; Stark et al. 2007). Although gravitational lensing technique can probe very faint high-z galaxies that cannot be found in blank fields with the current facilities (Stark et al. 2007; Bradley et al. 2008; Bouwens et al. 2009a; Zheng et al. 2009), these pencil beam surveys suffer from large uncertainties due to cosmic variance, and miss a population of bright galaxies at $z > 7$, which plays an important role in determining UV luminosity density for cosmic reionization and in understanding forming massive galaxies in their major star formation phase.

Motivated by this, we have conducted a wide-field z-dropout galaxy survey by performing deep z'- and y-band imaging down to $y = 26.0$ with *Subaru*/Suprime-Cam (Miyazaki et al. 2002), exploiting the excellent red sensitivity of the wide-field optical camera mounted on the 8.3m *Subaru Telescope*. Our program realizes a very large volume survey for z-dropout galaxies with the reasonably deep magnitude limit, which strongly constrains the bright end of UV LF at $z = 7$. In this paper, we present our bright z-dropout galaxy candidates found by our *Subaru* observations, and constrain cosmic star formation history and reionization in conjunction with faint z-dropout galaxies identified by the recent deep *HST*/WFC3 studies. We describe our observations and $z = 7$ z-dropout galaxy samples in Sections 2 and 3, respectively. We show the UV LF and UV luminosity density of $z = 7$ galaxies in Section 4. We discuss the cosmic star formation history, cosmic reionization, and the distribution of our z-dropout galaxies in Section 5; and summarize our results in Section 6. Throughout this paper, magnitudes are in the AB system. We adopt $(h, \Omega_m, \Omega_\Lambda, \Omega_b h^2, n_s, \sigma_8) = (0.7, 0.3, 0.7, 0.02, 1.0, 0.9)$.

2. DATA

2.1. Observations and Data Reduction

We carried out deep y- and z'-band imaging survey with Suprime-Cam in the Subaru Deep Field (SDF; Kashikawa et al. 2004) and GOODS-N (Giavalisco et al. 2004a) during the last three years from 2006 to 2009. The y band is a custom broadband filter centered at 1 μm. This filter was originally made for identifying $z \simeq 6$ galaxies by the two-color Lyman break selection technique (Shimasaku et al. 2005). Although this filter was formerly called z_R filter in Shimasaku et al. (2005), we refer to it as y filter for sake of simplicity. Figure 1 shows the total response of the y-band filter (central wavelength of 9860 Å and FWHM of 590 Å), which includes the CCD quantum efficiency, transmission+reflection of telescope+instrument optics, and atmospheric absorption. Each of SDF and GOODS-N field is covered by one pointing of Suprime-Cam whose field of view (FOV) is 918 arcmin^2. Table 1 summarizes our observations and the y and z' data that we used. Before 2007, we took y data with MIT-Lincoln Laboratory (MIT-LL) CCDs installed in Suprime-Cam (Miyazaki et al. 2002), while 2009 data were acquired with the new fully depleted Hamamatsu CCDs (Kamata et al. 2008). In our analysis, we also use archival y and z' images taken

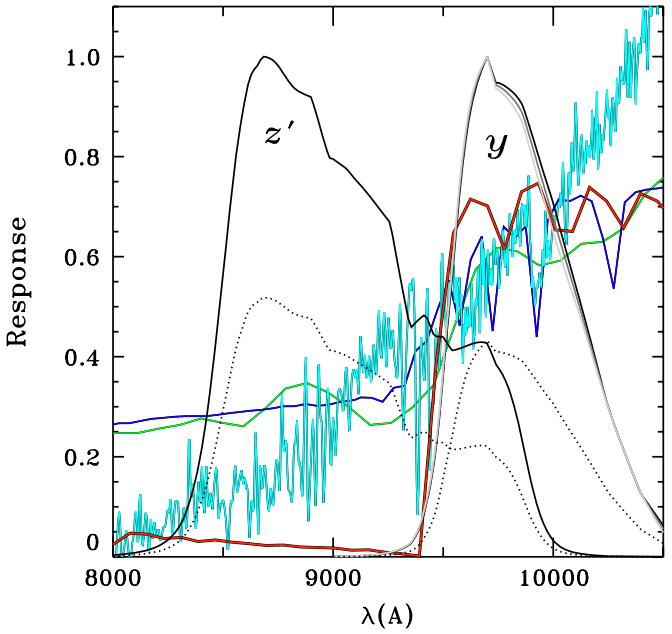

Figure 1. Response curves of y and z' bands, together with model spectra of a $z \sim 7$ galaxy and foreground interlopers. Black solid lines represent the response curves whose peaks are normalized to 1.0, while the black dotted lines denote those showing the total system throughput. Dark and light gray lines are the normalized total y-band response curves for the flux-weighted SDF and GOODS data. All of these response curves include the CCD quantum efficiency, transmission+reflection of telescope+instrument optics, and atmospheric absorption. Red line is the model spectrum mimicking the one of a typical dropout galaxy (Papovich et al. 2001), but redshifted to $z = 6.73$. Green line is a template spectrum of the typical local elliptical (old) galaxy placed at $z = 1.4$ (Coleman et al. 1980). Because the age of the universe at $z = 1.4$ is only 4–5 Gyr, which is younger than the typical age of local ellipticals, the oldest galaxies at $z = 1.4$ are probably younger than the local elliptical of this template. Thus, even the oldest galaxies at $z = 1.4$ should have a bluer SED than this elliptical template. Blue line plots a dusty-starburst spectrum at $z = 1.5$, which is a reproduction of the typical dusty-starburst SED (Cimatti et al. 2002). Cyan line shows a Galactic T3 dwarf star, one of the reddest Galactic dwarf stars (Knapp et al. 2004).

in 2001–2006 to make the deepest stacking of y and z' data available in SDF and GOODS-N. The total integration time of our y-band images are 26 and 33 hr in SDF and GOODS-N, respectively. The z' image of SDF is produced via a number of variable object studies such as supernovae (Poznanski et al. 2007), active galactic nuclei (AGNs; T. Morokuma et al. 2009, in preparation), and high proper motion stars (Richmond et al. 2009).

Our data were reduced using Suprime-cam Deep Field REDuction package (SDFRED; Yagi et al. 2002; Ouchi et al. 2004). We have found that the total throughput in the y band is improved by nearly a factor of 2 in 2009 with the new Hamamatsu CCDs, but that the shapes of y-band total response curves are almost identical between the data of MIT-LL (taken before 2007) and Hamamatsu CCDs (taken in 2009; Figure 1). Thus, we combine these y-band data taken with MIT-LL and Hamamatsu CCDs. Figure 1 displays the normalized total y-band response curves of the Hamamatsu CCDs and the flux-weighted MIT-LL+Hamamatsu CCDs for the SDF and GOODS data. The differences between all the response curves are negligibly small. Since we find a very small difference of $\lesssim$0.02 mag between the response curves of flux-weighted SDF and GOODS-N even with the model spectra of extremely red objects such as L/T dwarf stars and z-dropout galaxies (Section 4), we only use the y-band response curve of the flux-weighted SDF in our analysis. The

Table 1
Summary of Imaging Observations and Data

Field	Band	CCD	t_{exp} (s)	PSF Size[a] (arcsec)	Area (arcmin^2)	m_{lim}[b] (3σ AB mag)	Date of Observations and Note
SDF	y	MIT-LL	50614	...	...	...	2007 Apr 17–20, (2003 Jul 2, 2004 Mar 19–20)[c]
	y	Hamamatsu	43901	...	...	...	2009 Apr 24–26
	y	(Total)	94515	0.79 (0.99)	810	26.4	...
	z'	MIT-LL	104069	0.91 (0.99)	810	27.7	Data from T. Morokuma et al. (2009, in preparation)[d]
GOODS-N	y	MIT-LL	89308	...	...	...	2006 Apr 1, 3; 2007 Apr 17–18, 20
	y	Hamamatsu	29101	...	...	...	2009 Apr 24–25, 27
	y	(total)	118409	0.87 (0.87)	758	26.2	...
	z'	MIT-LL	39150	0.87 (0.87)	758	26.9	2007 Apr 19, (2001 Apr 20, 22; 2003 Apr 6; 2004 Mar 16; 2006 Feb 23–24)[c]

Notes.
[a] The FWHM of PSFs in the reduced image. The values in parenthesis indicate the FWHM of PSFs that are matched with broadband images in each field.
[b] The limiting magnitude defined by a 3σ sky noise level in a 1.″8-diameter circular aperture.
[c] The observation dates in parenthesis are those of the *Subaru* archival data taken by the other teams.
[d] See Section 2.

3σ sky noise of the reduced images are $(y, z') = (26.4, 27.7)$ and (26.2, 26.9) magnitudes in a 1.″8-diameter circular aperture for SDF and GOODS-N, respectively.

We mask contaminated areas with halos of bright stars and CCD blooming or low signal-to-noise ratio (S/N) regions caused by dithering at around the edge of the FOV. The sky area after the masking is 810 and 758 arcmin^2 in SDF and GOODS-N, respectively. The total area is 1568 arcmin^2. The positions of y and z' are aligned based on hundreds of stellar objects commonly detected in both images. After the point-spread function (PSF) sizes of these images are matched, FWHM sizes of PSFs are estimated to be $\simeq$0.″91 and $\simeq$0.″87 in SDF and GOODS-N, respectively.

2.2. Matched Images

Except for the y and z' bands, we use the legacy ground-based deep optical imaging data for SDF (Kashikawa et al. 2004) and GOODS-N (Capak et al. 2004), and the deep *HST*/ACS v2.0 and *Spitzer*/IRAC v0.3 available for the central $\simeq$160 arcmin^2 field of GOODS-N (Giavalisco et al. 2004a; Dickinson et al. 2003).[14] These data are registered with stellar objects to match the coordinates of our Suprime-Cam y and z' images in SDF and GOODS-N. Table 2 summarizes all of imaging data used in our study. Again, the PSF sizes of our SDF y and z' images are matched to that of the public SDF images with a PSF FWHM of 0.″99. Note that the public ground-based GOODS-N data include *U*-, *V*-, and *R*-band images with a relatively poor seeing (FWHM $\simeq$ 1.″5). We cannot homogenize the seeing sizes of GOODS-N images without a significant loss of S/Ns of our y and z' images. Because our purpose of the *UBVR* photometry is not to measure a color defined by the same PSF+aperture but to confirm non-detections, we place the upper limits of detection with a large, 3″-diameter, aperture size for those *U*, *V*, and *R* images.

During the observations, we took images of spectrophotometric standard star of G191-B2B with y-band filter in GOODS-N (Oke 1990; Bohlin et al. 1995). The standard star was observed four times under photometric condition. We calculate photometric zero points from the standard star data. The photometric zero points of the other images, i.e., GOODS-N z', SDF y, and SDF z', are determined by matching the zero points with those of images taken by Capak et al. (2004), Shimasaku et al. (2005), and Kashikawa et al. (2004), respectively. We check these photometric zero points based on colors of stellar objects in our field and 175 Galactic stars calculated from spectra given in Gunn & Stryker (1983). We find that the colors of stellar objects in our data are consistent with those of Gunn & Stryker's (1983) stars within $\simeq$0.03 mag.

[14] Note that *HST*/ACS v2.0 data are significantly deeper than the previously released images.

Table 2
Limiting Magnitudes

Band	GOODS-N (1)	SDF (2)
U	26.9[a]	...
B	27.5	28.9
B_{435}	28.4	...
V	26.2[a]	28.1
V_{606}	28.6	...
R	26.5[a]	28.4
I or i'	26.5	28.1
i_{775}	27.9	...
z_{850}	27.6	...
z'[b]	26.9	27.7
y[b]	26.2	26.4
$m_{3.6}$	26.1	...
$m_{4.5}$	25.5	...
$m_{5.8}$	23.5	...
$m_{8.0}$	23.4	...
m_{24}	21.2	...

Notes. 3σ limiting magnitudes in GOODS-N (1) and SDF (2). The magnitudes are defined with a 1.″8-diameter aperture for the ground-based optical images (*UBVRizy*), except for the GOODS-N *U*, *V*, and *R*, data. We apply a 0.″2-diameter aperture for the *HST* images (B_{435}, V_{606}, i_{775}, z_{850}), and a 3.″0-diameter for the *Spitzer* 3.6 μm, 4.5 μm, 5.8 μm, 8.0 μm, and 24 μm images ($m_{3.6}$, $m_{4.5}$, $m_{5.8}$, $m_{8.0}$, m_{24}). The limiting magnitudes of *Spitzer* data include the offsets of aperture corrections (see the text).
[a] The detection limits of ground-based GOODS-N *U*, *V*, and *R* images are defined with a 3.″0-diameter aperture due to the relatively poor seeing sizes (FWHM $\simeq$ 1.″5; see the text).
[b] The 4σ detection limits of y magnitudes are 25.9 (GOODS-N) and 26.1 (SDF). The 2σ upper limits of z' magnitudes are 27.4 and 28.2 in GOODS-N and SDF, respectively.

3. CATALOGS AND SAMPLES

3.1. Photometric Catalogs

Source detection and photometry are performed using SExtractor (Bertin & Arnouts 1996). The y images are chosen for our source detection. We measure 1.″8-diameter aperture magnitudes, and define a z'–y color with these aperture magnitudes obtained by the dual image mode of SExtractor. We correct the magnitudes of objects for Galactic extinction of $E(B - V) = 0.018$ (SDF) and 0.012 (GOODS-N; Schlegel et al. 1998). A total of 63,740 and 55,559 objects are identified down to the 4σ detection limits in SDF ($y = 26.1$) and GOODS-N ($y = 25.9$), respectively.

3.2. Photometric Samples

We isolate z-dropout galaxy candidates at $z \sim 7$ from foreground interlopers with our photometric data. Figure 1 plots the model spectra of a $z \sim 7$ galaxy as well as red objects including low-z galaxies and one of the reddest T dwarf stars (Knapp et al. 2004), which are likely to be prominent interlopers in our photometric sample. Figure 1 shows that the spectral feature of a significant 1216 Å trough for $z \sim 7$ galaxies is clearly different from the spectral shapes of foreground objects at the z'- and y-band wavelengths.

In Figure 2, we present predicted z'–y colors as a function of redshift for these model spectra. This figure demonstrates that no objects except $z \sim 7$ galaxies and some late-type dwarf stars have colors redder than z'–$y \gtrsim 1.5$. Since the wavelength coverages of z' and y bands are very close (Figure 1), the Lyα trough of $z \sim 7$ galaxies can be more clearly distinguished from the red continuum of foreground objects. Indeed, the elliptical galaxy of Coleman et al. (1980) is bluer than $z \gtrsim 6.5$ galaxies by $\Delta(z'$–$y) \gtrsim 0.4$–0.5 even at its reddest color. A strong z'–y color cut can isolate $z \sim 7$ galaxies with a small fraction of foreground interlopers. On the other hand, the recent studies of $z \sim 7$ galaxies apply a relatively weak color criterion for the Lyα trough, e.g., z'–$Y_{105} \gtrsim 1$ or z'–$J_{110} \gtrsim 1$, with a broad band of Y/J whose central wavelength is redder than that of our y band (Bouwens et al. 2008; Oesch et al. 2009b; Bunker et al. 2009; Castellano et al. 2009; Hickey et al. 2009). The colors of z'–$Y_{105} \sim 1$ and z'–$J_{110} \sim 1$ fall below the red peaks of the Coleman et al.'s (1980) elliptical galaxy (see, e.g., Figure 2 of Bunker et al. 2009), and these studies cannot remove such foreground red galaxies with a z'–Y_{105} or z'–J_{110} color alone. Instead, these studies can distinguish foreground red galaxies with their available deep NIR (J, H, and/or K) photometry (e.g., Figure 3 of Bunker et al. 2009). The idea of our candidate selection is to discriminate foreground red galaxies without NIR photometry but with a color cut stronger than the color criterion of the other studies. In addition to a Lyα trough, a rest-frame far UV continuum below Lyman break (912 Å) is damped by intergalactic medium (IGM) absorption with a large Lyman continuum opacity (Inoue & Iwata 2008). Because no such continuum should be identified at a wavelength shorter than 7000($\simeq 912 \times [1 + 6.7]$) Å for sources at $z \gtrsim 6.7$, nondetection criteria should be given in U, B, V, and R bands whose bandpasses are bluer than 7000 Å. From the model colors and the lack of a far UV continuum, we define the selection criteria of $z \sim 7$ galaxies:

$$z' - y > 1.5, \quad U > U_{2\sigma}, \quad B > B_{2\sigma}, \quad V > V_{2\sigma}, \quad R > R_{2\sigma}, \tag{1}$$

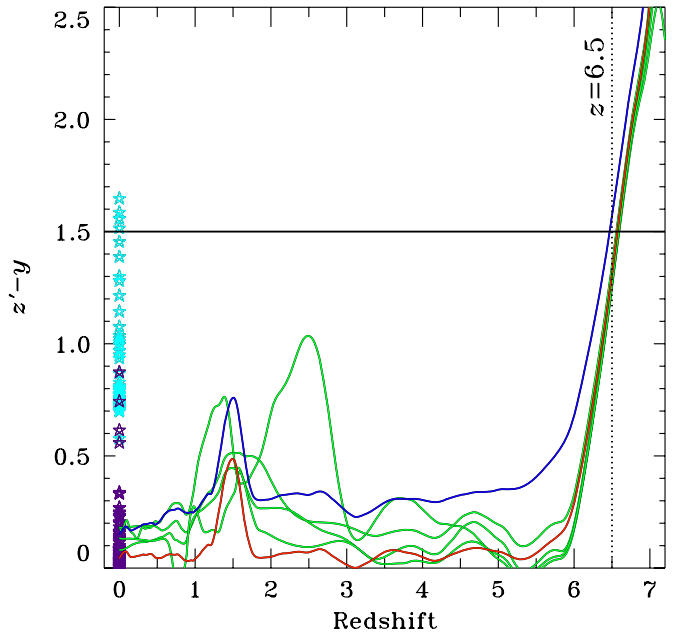

Figure 2. Colors of z'–y for various objects as a function of redshift. Red and blue lines represent the models of dropout and dusty-starburst galaxies that are reproductions of the typical SEDs shown in Papovich et al. (2001) and Cimatti et al. (2002), respectively. Green lines indicate elliptical, Sbc, Scd, and irregular galaxies (Coleman et al. 1980). Purple and cyan star marks are Galactic stars (Gunn & Stryker 1983) and L1-L9/T0-T9 dwarf stars (Knapp et al. 2004). Black solid line indicates our color selection criterion, z'–$y > 1.5$. The black dotted line marks a redshift, $z = 6.5$, that is roughly a lower limit of our selection.

where $U_{2\sigma}$, $B_{2\sigma}$, $V_{2\sigma}$, and $R_{2\sigma}$ are the 2σ limiting magnitudes of U, B, V, and R images, respectively. The U-band criterion is only applied to the objects in GOODS-N, since there are no public U-band data in SDF. The 2σ limiting magnitudes are $(B_{2\sigma}, V_{2\sigma}, R_{2\sigma}) = (29.4, 28.6, 28.8)$ in SDF and $(U_{2\sigma}, B_{2\sigma}, V_{2\sigma}, R_{2\sigma}) = (27.3, 28.0, 26.7, 27.0)$ in GOODS-N. We select $z \sim 7$ galaxy candidates with these photometric criteria down to the 4σ limits of $y = 26.1$ and $y = 25.9$ in SDF and GOODS-N, respectively. Note that the color criterion of z'–$y > 1.5$ can be securely applied to our photometric catalogs down to the given y-band detection limits, because the 2σ upper limits of z' images reach 28.2 (SDF) and 27.4 (GOODS-N). Our candidate selection is made with the photometric catalogs of Suprime-Cam images alone both in SDF and GOODS-N. Although deep *HST* images are available in the central ~160 arcmin^2 field of GOODS-N, we do not use these *HST* images at this stage to avoid making a heterogeneous sample given by the different detection limits on the sky of GOODS-N. Instead, we take advantage of the deep *HST* images for confirming nondetections of blue continuum for the candidates falling in the area with the *HST* images (see below).

After we reject spurious sources near the spikes of bright sources, the residuals of sky subtraction, etc., by visual inspection, we obtain z-dropout galaxy samples consisting of 15 and 7 candidates in SDF and GOODS-N, respectively. All of these candidates have magnitudes fainter than $y = 25.4$ and brighter than the detection limits in each field. Snapshots of these 22 candidates are displayed in Figure 3; and properties of our candidates are summarized in Table 3. Some of our candidates are detected in z' as well as y bands. Because the bandpass of z' band includes both red and blue sides of GP trough (1216 Å), the detections of faint z' counterparts are reasonable. The z'-band detections rather confirm that the candidates are neither spurious sources nor transients appearing in the y images. Al-

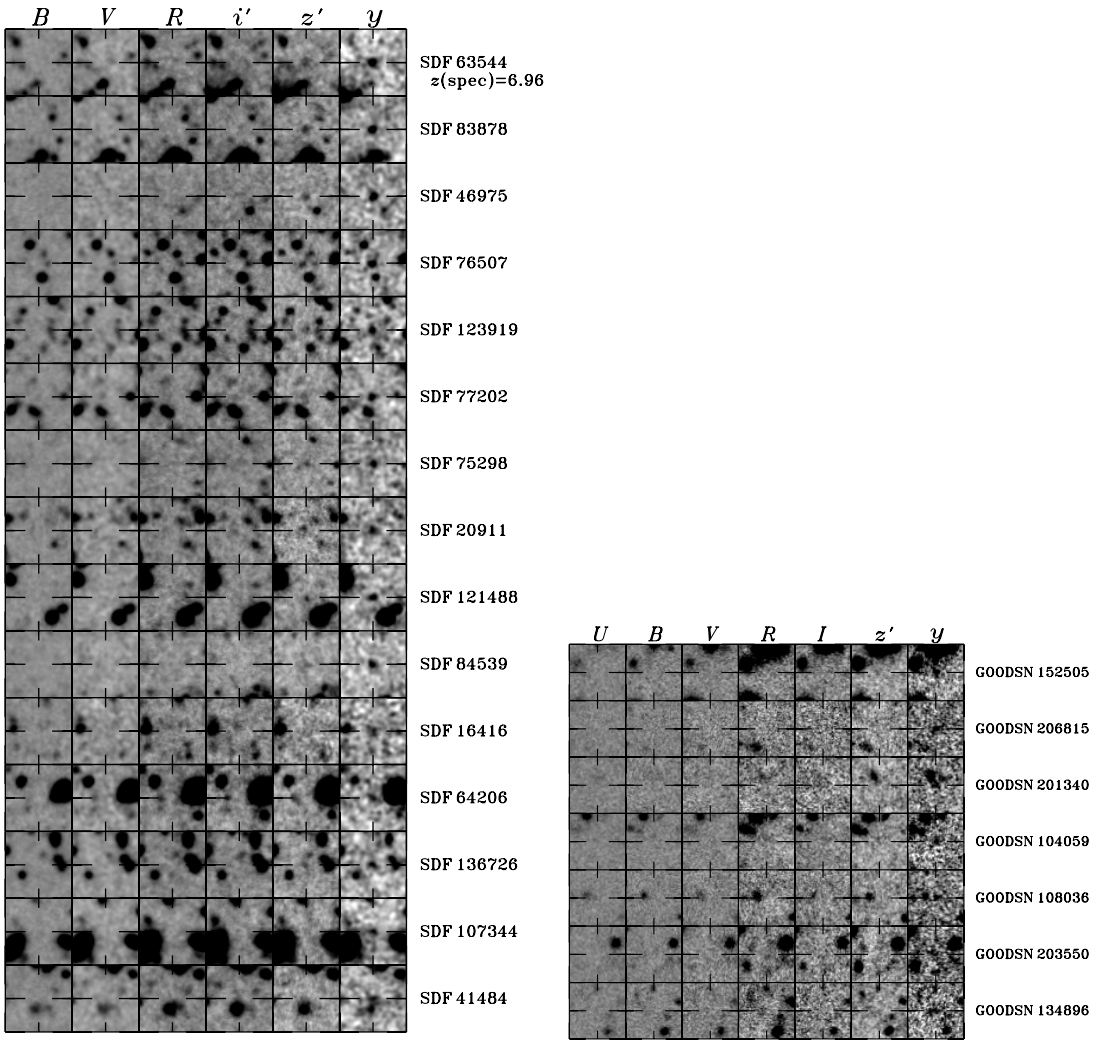

Figure 3. Snapshots of our z-dropout candidates identified in SDF (left panel) and GOODS-N (right panel). Each object has images of U, B, V, R, i', z', and y bands with an ID number on the right. The size of images is $10'' \times 10''$. North is up and east is to the left.

though we do not apply a criterion of non-detection in i'/I band where a UV continuum between Lyman break (912 Å) and GP trough (1216 Å) falls, none of our candidates have an i'/I-band counterpart with a flux beyond our detection limits.

We check the spectroscopic catalogs of SDF and GOODS-N, which are obtained by Kashikawa et al. (2003, 2006), Shimasaku et al. (2003, 2006), Ouchi et al. (2004), Yoshida et al. (2006), Iye et al. (2006), Nagao et al. (2007), Hayashi et al. (2009), and Ly et al. (2009) for SDF, and Wirth et al. (2004), Reddy et al. (2006), Barger et al. (2008), Cohen et al. (2000); Cohen (2001), Steidel et al. (1996, 1999, 2003), Phillips et al. (1997), Lowenthal et al. (1997), and Dawson et al. (2001) for GOODS-N. We find that one of our z-dropout candidates, SDF-63544, has a spectroscopic redshift of $z = 6.96$, which was originally identified by Iye et al. (2006) in their Lyα emitter (LAE) study. SDF-63544 is the first dropout galaxy at $z \simeq 7$ with a spectroscopic redshift. This object has a y-band magnitude of $y = 25.42$, which is the brightest candidate in our z-dropout galaxy samples. It should be noted that our photometric sample surely includes a real $z \simeq 7$ galaxy. On the other hand, we also find that none of our candidates are low-z objects with a spectroscopic redshift. This confirms that our photometric criteria do not select obvious foreground objects.

Two out of seven candidates in the GOODS-N field, GOODSN-152505 and GOODSN-108036, fall in the region with the deep GOODS-N *HST*/ACS and *Spitzer* images. We display snapshot images in Figure 4. We have found that neither candidate is detected in *HST*/ACS B_{435}, V_{606}, and i_{775} bands.[15] The *Spitzer* images of GOODSN-152505 and GOODSN-108036 are confused by the nearby bright objects due to large PSF sizes in IRAC and MIPS data. However, there are some signatures of possible counterparts for GOODSN-152505 in the 4.5 μm band and for GOODSN-108036 in the 3.6 μm and 4.5 μm bands, which would be different from the effects of source confusion. Although photometry of these possible *Spitzer* counterparts are more or less contaminated by fluxes of the nearby objects, we simply calculate total magnitudes from 3″-diameter aperture magnitudes and aperture corrections for IRAC and MIPS fluxes given in Yan et al. (2005) and the *Spitzer* web page,[16] respectively. Since these sources are confused by the nearby objects, we find that total magnitudes ($m_{3.6}$,$m_{4.5}$) of GOODSN-152505 and GOODSN-108036 are fainter than (23.4, 24.2) and (24.8,24.4), respectively. Thus, the colors of y–$m_{3.6}$ and y–$m_{4.5}$ are $\lesssim$1–2 and $\lesssim$1. Because Eyles et al. (2007) report that their $z \sim 6$ galaxies with the IRAC detections have colors of 1–2 mag in z'–$m_{3.6}$ and z'–$m_{4.5}$ (as well

[15] GOODSN-152505 is located near the edge of *HST* GOODS-N field, and not covered by the B_{435} image.
[16] http://ssc.spitzer.caltech.edu/mips/apercorr/

Table 3
$z = 7$ Galaxy Candidates

ID	U	B	V	R	I/i	z	y	$m_{3.6}$	$m_{4.5}$	$z'-y$	z(spec)	Note
					GOODS-N							
GOODSN-152505[a]	>27.3	>28.0 (>28.4)	>26.7 (>28.6)	>27.0	>27.0 (>27.9)	>27.4 (>27.6)	25.50	>23.4[b]	>24.2[b]	>1.90	...	Source confusion in *Spitzer* bands
GOODSN-206815	>27.3	>28.0	>26.7	>27.0	>27.0	>27.4	25.52	...	...	>1.88	...	...
GOODSN-201340	>27.3	>28.0	>26.7	>27.0	>26.9[b]	>27.4	25.69	...	...	>1.71	...	Source confusion
GOODSN-104059	>27.3	>28.0	>26.7	>27.0	>27.0	>27.4	25.79	...	...	>1.61	...	...
GOODSN-108036[a]	>27.3	>28.0 (>28.4)	>26.7 (>28.6)	>27.0	>27.0 (>27.9)	>27.4 (>27.6)	25.82	>24.8[b]	>24.4[b]	>1.58	...	Weak source confusion in *Spitzer* bands
GOODSN-203550	>27.3	>28.0	>26.7	>27.0	>27.0	>27.4	25.83	...	...	>1.57	...	Spurious source?
GOODSN-134896	>27.3	>28.0	>26.7	>27.0	>27.0	>27.4	25.86	...	...	>1.54	...	...
					SDF							
SDF-63544	...	>29.4	>28.6	>28.8	>28.6	27.02	25.42	...	...	1.60	6.96	Spectrum shown in Iye et al. (2006)
SDF-83878	...	>29.4	>28.6	>28.8	>28.6	27.04	25.49	...	...	1.55	...	...
SDF-46975	...	>29.4	>28.6	>28.8	>28.6	27.48	25.51	...	...	1.97	...	...
SDF-76507	...	>29.4	>28.6	>28.8	>28.6	27.11	25.59	...	...	1.52	...	...
SDF-123919	...	>29.4	>28.6	>28.8	>28.6	27.51	25.79	...	...	1.72	...	...
SDF-77202	...	>29.4	>28.6	>28.8	>28.6	27.50	25.86	...	...	1.64	...	...
SDF-75298	...	>29.4	>28.6	>28.8	>28.6	27.50	25.87	...	...	1.63	...	...
SDF-20911	...	>29.4	>28.6	>28.8	>28.6	27.41	25.89	...	...	1.52	...	...
SDF-121488	...	>29.4	>28.6	>28.8	>28.6	27.49	25.97	...	...	1.52	...	...
SDF-84539	...	>29.4	>28.6	>28.8	>28.6	28.16	25.98	...	...	2.18	...	...
SDF-16416	...	>29.4	>28.6	>28.8	>28.6	>28.2	25.99	...	...	>2.21	...	...
SDF-64206	...	>29.4	>28.6	>28.8	>28.6	>28.2	26.07	...	...	>2.13	...	...
SDF-107344	...	>29.4	>28.6	>28.8	>28.6	>28.2	26.08	...	...	>2.12	...	...
SDF-136726	...	>29.4	>28.6	>28.8	>28.6	27.59	26.08	...	...	1.51	...	...
SDF-41484	...	>29.4	>28.6	>28.8	>28.2[b]	28.05	26.09	...	...	1.96	...	Source confusion

Notes. The upper limits in the ground-based images, *UBVRIizy*, are defined by the 2σ level. The numbers in parenthesis are 3σ upper limits of *HST*/ACS B_{435}, V_{606}, i_{775}, and z_{850} bands.

[a] Our candidates falling in the central ~160 arcmin^2 field of GOODS-N with *HST* and *Spitzer* images. There are no obvious counterparts in IRAC 5.8 μm, 8.0 μm, and MIPS 24 μm bands (see Figure 4). The 3σ upper limits in these bands are ($m_{5.8}$, $m_{8.0}$, m_{24}) = (23.5, 23.4, 21.2).

[b] Fluxes of these objects are contaminated by close bright objects on the sky.

as J–$m_{3.6}$ and J–$m_{4.5}$; see also Yan et al. 2005, 2006), the colors of our two candidates are comparable to those of $z \sim 6$ galaxies. This confirms that these two candidates are not extremely red galaxies at $z \sim 2$–3, such as reported by Yan et al. (2004), whose optical to IRAC colors (z–$m_{3.6}$) exceed 3.3. Although the possible IRAC counterparts of our z-dropout galaxy candidates would indicate that there exist post-starburst galaxies even at $z \sim 7$, there remains the possibility that these two candidates are foreground interlopers. We will discuss stellar population of these two candidates via detailed spectral energy distribution model fitting after we confirm the redshifts of these candidates by spectroscopy.

There are no obvious counterparts of these two candidates at longer wavelengths: IRAC 5.8 μm, 8.0 μm, and MIPS 24 μm bands. The MIPS snapshot of GOODSN-152505 shows a source at the left side, but this MIPS source is a counterpart of a bright source located near the left corner. Because the detection limits of the three bands are too shallow (21–23 mag; Table 2) to identify galaxies at large distances, the non detections, again, confirm that these two candidates are neither extremely red galaxies nor AGN at low redshifts.

4. LUMINOSITY FUNCTION

4.1. Surface Number Densities and Detection Completeness

We obtain the number counts of all y-band detected objects, $N_{\rm all}(m)$, and our z-dropout galaxy candidates, $N_{\rm cand}(m)$, from our photometric catalogs. We calculate the surface number densities, $\Sigma_{\rm obs}$, by dividing $N_{\rm all}(m)$ and $N_{\rm cand}(m)$ by our respective survey areas. The results are presented in the bottom panel of Figure 5. Since the surface number densities of faint objects are affected by detection incompleteness, we estimate detection completeness as a function of y magnitude by Monte Carlo simulations. We distribute 7240 artificial objects with a PSF on our y-band images after adding photon Poisson noise, and detect them in the same manner as for the detection for our photometric catalogs with SExtractor. We repeat this process 20 times, and compute the ratio of recovered objects to the input objects. The top panel of Figure 5 shows the detection completeness of our y-band images. We find that the detection completeness is typically $\gtrsim$70% for relatively luminous sources with $y \lesssim 25.5$. The detection completeness is $> 50\%$ even in the faintest magnitude bins centered at $y = 25.85$ (SDF) and $y = 25.65$ (GOODS-N). We correct the surface number densities for the detection completeness, and present them in the bottom panel of Figure 5.

4.2. Contamination

There are four sources of contamination in our $z \sim 7$ galaxy samples: (1) spurious y-band sources made of noise fluctuations; (2) transients, such as faint variable stars+AGN and supernovae detected in our y-band images; (3) foreground red objects entering our samples due to photometric errors; and (4) L/T dwarf stars satisfying our color selection criteria. We define the numbers of contamination for (1), (2), (3), and (4) in our samples as $N^1_{\rm cont}(m)$, $N^2_{\rm cont}(m)$, $N^3_{\rm cont}(m)$, and $N^4_{\rm cont}(m)$, respectively. Below, we check the effects of contamination, and estimate their impacts on our z-dropout galaxy samples.

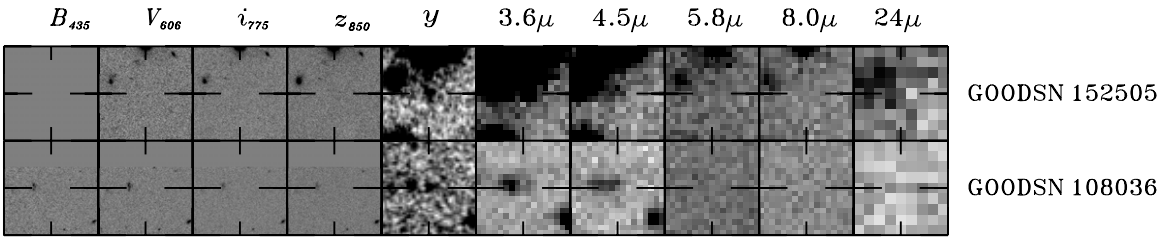

Figure 4. Snapshots of two z-dropout candidates falling in the area with the *HST* and *Spitzer* images in GOODS-N. From left to right, we display *HST*/ACS B_{435}, V_{606}, i_{775}, z_{850}, Suprime-Cam y, *Spitzer*/IRAC 3.6 μm, 4.5 μm, 5.8 μm, 8.0 μm, and *Spitzer*/MIPS 24 μm images. The Suprime-Cam y image is shown for comparison. GOODSN-152505 is not covered with the B_{435} image. The size of all images is $10''\times10''$, but that of 24 μm band is $11''\times11''$. North is up and east is to the left.

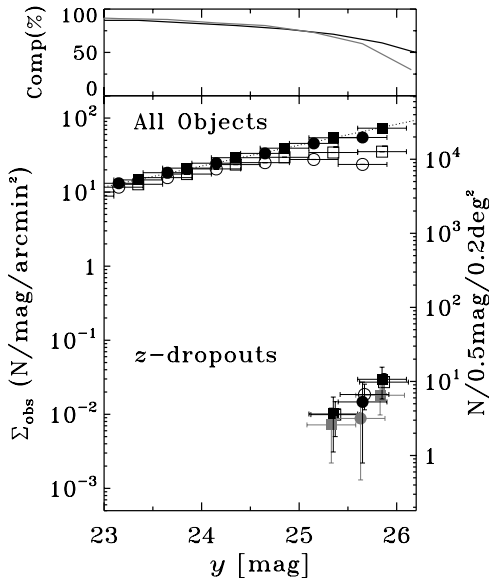

Figure 5. Top panel: detection completeness of our y-band images in percentage. Black and gray solid lines represent the completeness for 1.″8-diameter aperture photometry in SDF and GOODS-N, respectively. Bottom panel: surface densities of our objects detected in our y data. Lower and upper sequences of points show surface densities of our z-dropout galaxy candidates and all objects detected in the y images, respectively. The surface densities are shown with the squares (SDF) and circle (GOODS-N). In the upper sequence, filled black symbols are those with the completeness correction, while open symbols are not applied for the correction. In the lower sequence, filled gray symbols are surface densities that are subtracted with the numbers of contamination, and filled black symbols denote the best estimate of our z-dropout galaxy surface densities with both the contamination and completeness corrections (see Section 4). We present total magnitudes from SExtractor's MAG_AUTO for the upper sequence to obtain the unbiased magnitude surface density relation. Although the photometry of z-dropout galaxies is carried out with a 1.″8-diameter aperture to maximize the signal-to-noise ratio of faint sources, the aperture corrections are applied for z-dropout galaxies in the LF plot of Figure 7. For the presentation purpose, we slightly shift the open and gray points along the abscissa. The exact magnitudes are the same as magnitudes of black filled points. The vertical axis on the right side indicates the number counts of objects, i.e., $N/(0.5\ \mathrm{mag})/(0.2\ \mathrm{deg}^2)$, which approximately correspond to numbers of z-dropout galaxies identified in each target field. Dotted line represents the best-fit power law to the completeness-corrected surface densities of all objects.

1. *Spurious sources:* Because we push our y-band detection limits, our $z\sim7$ galaxy samples may include spurious sources made of noise peaks. Some of these y-band spurious sources could pass our selection criteria of Equation (1). To estimate how much spurious sources are included in our z-dropout galaxy samples, we carry out source detection and color selection same as those in Section 3, but with images whose ADU counts are multiplied by -1. We run SExtractor with these negative-count images, and make negative y-band detection catalogs. We apply the color criteria of Equation (1), and reject sources apparently made by the residuals of sky subtraction in the same manner as for the real z-dropout galaxy selection. We find 0 and 1 spurious $z\sim7$ galaxy candidate in the negative SDF and GOODS-N images, respectively. We conclude that our samples include $N^1_{\rm cont}(m)=0$ (SDF) and 1.0 ± 1.0 (GOODS-N) spurious source statistically, where the error is estimated by Poisson statistics.
2. *Transients:* Although our y images are the stacked data that were acquired in a 6 yr (3 yr) long period from 2003 (2006) to 2009 for SDF (and GOODS-N; see Table 1), we investigate the possibility of transients for our z-dropout candidates. We stack y data taken before and after 2008, and obtain y-band images for the two epochs. The y-band detection limits of the former ($y_{\rm lim}^{\rm epoch1}$) and the latter ($y_{\rm lim}^{\rm epoch2}$) images are ($y_{\rm lim}^{\rm epoch1}$, $y_{\rm lim}^{\rm epoch2}$) =(25.9, 26.2) in SDF and (26.0, 25.6) in GOODS-N. We have carried out photometry at the positions of our z-dropout galaxy candidates, and found no candidates detected at the 3σ levels that show a significant magnitude change between these two epochs by $\gtrsim$0.5 mag (corresponding to 1σ–2σ). Thus, we conclude $N^2_{\rm cont}(m)=0$ in both SDF and GOODS-N. Checking this result, we calculate an expected number of transients based on the deep and wide-field transient study results of Morokuma et al. (2008). Morokuma et al. (2008) present that the number density of transients (with the timescale greater than 200 days) in the magnitude range of $i'\simeq25.4$–26.0 is $\simeq0.4/\mathrm{deg}^2$ Assuming the difference of magnitudes between y and i' is negligible for transients which are mostly nearby objects, the expected number of transients in our SDF and GOODS-N samples is only $\sim$0.1 with the detection completeness correction. This estimate is consistent with our conclusion of no transients in our z-dropout galaxy samples.
3. *Foreground red objects entering our samples due to photometric errors:* It is possible that some foreground objects, such as red galaxies at intermediate redshifts, enter our color criteria by photometric errors, although their intrinsic colors cannot satisfy the criterion of $z-y>1.5$. We make an input mock catalog mimicking foreground objects, and carry out Monte Carlo simulations with the mock catalog to estimate the numbers of foreground interlopers. The mock catalog has the same number density distribution as that of all y-detected objects corrected for the detection completeness (filled circles at the upper sequence in the bottom panel of Figure 5). In the mock catalog, colors of the bright ($y<24.5$) objects are the same as those of the observed y-detected objects. Because faint objects have moderately large photometric errors, we do not use colors of objects with a magnitude fainter than $y=24.5$. Instead, we assign color distribution of observed y-detected objects with $y=23.5$–24.5 to the objects with $y>24.5$ in the mock

catalog. Then, we perform Monte Carlo simulations in the same manner as Section 4.1; distributing artificial objects from the mock catalog on our real images and detecting them with SExtractor. We find that expected numbers of these interlopers are $N^3_{\rm cont}(m) = 0.85$ in SDF down to $y = 26.1$, and 0.80 in GOODS-N down to $y = 25.9$.

4. *L/T dwarf stars:* Figure 2 indicates that none of foreground objects except Galactic late-type stars can satisfy our color criterion of $z–y > 1.5$without photometric errors. Late-type stars are potentially the largest source of contamination in our z-dropout galaxy samples. Estimating the numbers of late-type stars which contaminate our z-dropout samples, we carry out Monte Carlo simulations same as (3), but with an input mock catalog of late-type stars. We use the number density of L/T dwarfs as a function of Galactic latitude presented in Ryan et al. (2005) who derive the number densities in 15 deep *HST*/ACS fields down to $z = 26.0$ at various Galactic latitude and fit them to the model of surface density averaged over Galactic longitude. The colors of L/T dwarfs are calculated with the spectral templates of Knapp et al. (2004) that cover L1–L9 and T0–T9 stars. The results of these Monte Carlo simulations show that the numbers of late-type star contaminants are $N^4_{\rm cont}(m) = 5.35$ down to $y = 26.1$ in SDF, and 2.80 down to $y = 25.9$ in GOODS-N. The uncertainties of these simulation results are 0.4–0.5 in number.

4.3. Redshift Distribution

We have estimated redshift distribution of our z-dropout galaxies, $C(m, z)$, by Monte Carlo simulations with an input mock catalog of high-z galaxies. The mock catalog consists of high-z galaxies whose properties are given with the probability distributions of (1) number count, (2) continuum color, and (3) Lyα emissivity. First, for the probability distribution of (1), we use the surface number densities of our z-dropout galaxies corrected for contamination and completeness (black filled points in Figure 5). Second, we assume that high-z galaxies have the average UV continuum slope of $\beta = -2$, which is found in $z \sim 6$ dropout galaxies (Stanway et al. 2005; Yan et al. 2005; Bouwens et al. 2006, 2007, 2009c), and that the probability distribution of β is a Gaussian function with a standard deviation of $\sigma_\beta = 0.5$. We generate spectra with the stellar population synthesis model of Bruzual & Charlot (2003), and obtain galaxy spectra with $\beta = (-3.0)$–(-1.0). The model parameters are the same as those of the average values estimated for Lyman break galaxies (LBGs) at $z = 3$ (Papovich et al. 2001), but with a young age of 4 Myr and Calzetti dust extinction ranging from $E(B - V) = 0.008$ to 0.400, so that we can reproduce a set of spectra covering from the very blue ($\beta = -3.0$) to the moderately red ($\beta = -1.0$) continua. We apply a GP optical depth calculated from Madau (1995) for the IGM absorption, and use this probability distribution for (2). Third, for the fraction of Lyα emitting galaxies, we assume that 30% of $z = 7$ dropout galaxies have a Lyα emission line with a rest-frame equivalent width ($\rm EW_0$) of > 20 Å, which is the same as the estimates for $z = 6$ dropout galaxies down to $\sim L^*$ (Stanway et al. 2004a, 2004b, 2007; Vanzella et al. 2006; Dow-Hygelund et al. 2007). We add a Lyα luminosity to these 30% of dropout galaxies with the $\rm EW_0$ probability distribution of LAEs at $z = 5.7$ derived by Ouchi et al. (2008). Since Shapley et al. (2003) have found that about 50% of their $z = 3$ LBGs have a Lyα $\rm EW_0$ of $\leqslant 0$ Å, we assume that a half of our $z = 7$ dropout galaxies have no Lyα emission line. For the rest of 20% of high-z galaxies, we add a very weak $\rm EW_0 = 0$–20 Lyα line to their spectra.

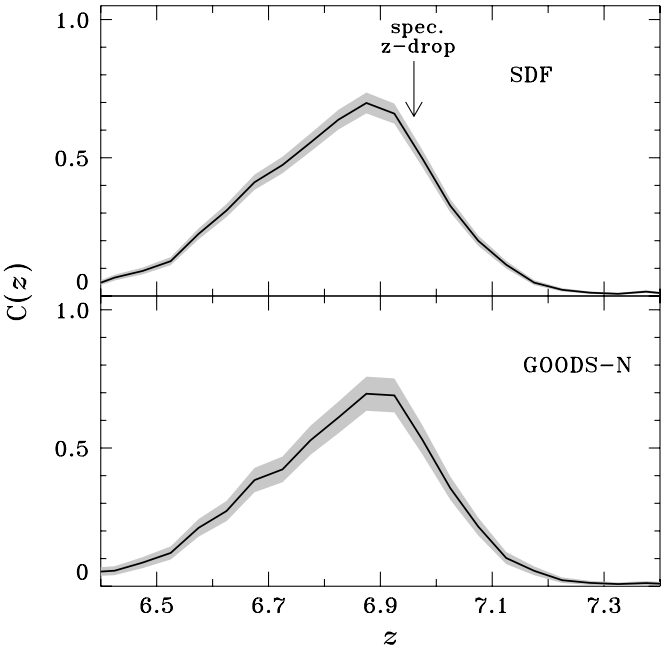

Figure 6. Redshift distribution of our z-dropout galaxies in SDF (top) and GOODS-N (bottom). Solid lines plot the redshift distributions averaged over magnitudes weighted with the number density distributions of our z-dropout galaxies. Gray shades represent errors of the redshift distribution estimates obtained by our Monte Carlo simulations. Arrow indicates the redshift of our z-dropout galaxy with the spectroscopic confirmation (SDF-63544; $z_{\rm spec} = 6.96$).

Finally, we produce an input mock catalog of high-z galaxies that are distributed in the redshift space homogeneously, and apply statistical weights following the probability distributions of (1), (2), and (3) of Section 4.3 shown above. This mock catalog is used to carry out Monte Carlo simulations in the same manner as those in Section 4.2. Note that LF around the detection limits are usually overestimated because Poisson noise produces more sources with an up scattered flux than those with a down scattered flux at a given flux bin for objects with a typical steep source number count (Eddington 1940). To correct this bias, we extrapolate the relation between surface number density and magnitude down to $y = 27$, and produce the mock catalog including faint sources below our detection limit. We obtain y-band detection catalogs by the Monte Carlo simulations, and select artificial z-dropout galaxies with the color criteria (Equation (1)) to draw mock samples of z-dropout galaxies. We calculate the ratio of the selected objects to the input objects as a function of redshift, which corresponds to the redshift distribution of our z-dropout galaxies. Figure 6 plots the redshift distribution of our z-dropout galaxies, $C(z)$, averaged over magnitudes with the probability distributions of (1). For both data of SDF and GOODS-N, the peak redshift of $C(z)$ is $z = 6.9$; and 90 percent of the z-dropout galaxies fall in $z = 6.5$–7.1. Thus, the redshift window of our z-dropout selection is $z = 6.9^{+0.2}_{-0.4}$.

4.4. UV Luminosity Function

We derive the UV LF of z-dropout galaxies based on the numbers of our candidate galaxies (Section 4.1) and the contamination objects (Section 4.2), and the completeness as a function of redshift, i.e., redshift distribution (Section 4.3).

We calculate the number density, $n(m)$, of z-dropout galaxies at each field in a given magnitude bin by

$$n(m) = \frac{\left[N_{\rm cand}(m) - \sum_{i=1}^{n} N^{i}_{\rm cont}(m)\right]}{\int_0^\infty \frac{dV}{dz} C(m,z) dz}, \quad (2)$$

where n represents the four kinds of contaminants satisfying our selection criteria in a given magnitude bin ($n = 4$; see Section 4.2), and $\frac{dV}{dz}$ is the differential cosmic volume with an area of SDF or GOODS-N. Because we apply a 1.″8-diameter aperture for z-dropout galaxy photometry to maximize the S/N, we need to brighten the y magnitudes with an aperture correction to estimate total fluxes. On the other hand, our y-band magnitudes can be contaminated with Lyα emission lines. We should subtract the contributions of Lyα fluxes to obtain UV-continuum magnitudes, and dim the y-band brightness accordingly. Moreover, we should apply k-correction to get UV-continuum luminosities at the rest frame ∼1500 Å from our 1200–1300 Å luminosities including small portions of Lyα forest below GP trough, which enter the bandpass of our y filter. We estimate a correction factor to derive total UV-continuum magnitudes at ∼1500 Å from our y-band magnitudes based on the results of our Monte Carlo simulations in Section 4.3. We calculate the mean input 1500 Å-continuum and the output y-band magnitudes averaged with the statistical weights from the probability distribution functions (Section 4.3), and obtain correction magnitudes of +0.01 and +0.05for SDF and GOODS-N samples, respectively. We apply these small corrections to our UV-continuum magnitude estimates.

Figure 7 presents UV LF of z-dropout galaxies from our samples with the red filled squares (SDF) and circle (GOODS) as well as our upper limits with the red open circles. We also plot z-dropout galaxy UV LFs derived by the deep *HST* NICMOS+WFC3 (Bouwens et al. 2008; Oesch et al. 2009a, 2009b; McLure et al. 2009b) and the ground-based (Richard et al. 2006; Mannucci et al. 2007) studies, together with UV LFs at low redshifts.[17] Because we have a spectroscopically identified galaxy at $z = 6.96$, we can also place a lower limit on the UV LF. We estimate a 1500 Å-continuum magnitude of this galaxy to be $M_{\rm UV} = -21.40 \pm 0.31$ from the y-band photometry ($y = 25.42$), Lyα flux (2×10^{-17} erg s^{-1} cm^{-2}; Iye et al. 2006; Ota et al. 2008), and the mean model spectrum at $z = 6.96$ with $\beta = -2.0$ (Section 4.3). We show this lower limit with the magenta arrow in Figure 7.

Note that our study provides, for the first time, measurements of $z = 7$ UV LF at the bright magnitude of $-22 < M_{\rm UV} < -21$ as well as the lower limit based on the spectroscopically identified z-dropout galaxy. We find that our UV LF at $z = 7$ falls significantly below that at $z = 6$. Because our z-dropout galaxy samples are largely corrected for contamination estimated by the simulations (Section 4.2), these small number densities of our z-dropout galaxies could be due to overestimates of the contaminants. We derive UV LF of our z-dropout galaxies in the same manner as above, but with no contamination subtraction, and refer to these estimates as the maximal LF that provides conservative upper limits. We show the maximal LF with the magenta inverse-triangles in Figure 7. These magenta inverse-triangles also fall below the $z = 6$ UV LF measurements. Note that the $z = 6$ UV LF measurements would also have the similar problems in contamination estimates, but our magenta inverse-triangles come below the gray shade area in Figure 7 that represents a variance of $z = 6$ LFs derived by different studies with various contamination estimates. Thus, we conclude with our LF measurements and maximal LF estimates that $z = 7$ UV LF definitely decreases from $z = 6$ at the bright end. Our conclusion is consistent with the claim of Mannucci et al. (2007); Castellano et al. (2009). Moreover, this decreasing tendency is similar to that found at the faint magnitudes by the *HST* studies ($M_{\rm UV} > -21$; Bouwens et al. 2008; Oesch et al. 2009a, 2009b; McLure et al. 2009b; Bunker et al. 2009). The combination of our results and the *HST* studies suggests that UV LF decreases at both bright and faint magnitudes from $z = 6$ to 7. We fit a Schechter function to the LF measurements from our and the *HST* studies, and obtain the best-fit parameters of $\phi^* = 0.69^{+2.62}_{-0.55} \times 10^{-3}$Mpc^{-3}, $M^*_{\rm UV} = -20.10 \pm 0.76$ mag, and $\alpha = -1.72 \pm 0.65$ that maximize the likelihood, $\mathcal{L} = \Pi_i\ p[N_{\rm obs}(m_i), N_{\rm exp}(m_i; \phi^*, M^*_{\rm UV}, \alpha)]$, where $p[x, \mu]$ is the Gaussian distribution with a mean μ evaluated at x, and $N_{\rm obs}$ and $N_{\rm exp}$ are, respectively, the numbers of galaxies within a magnitude bin of m_i from observations and expectations for a

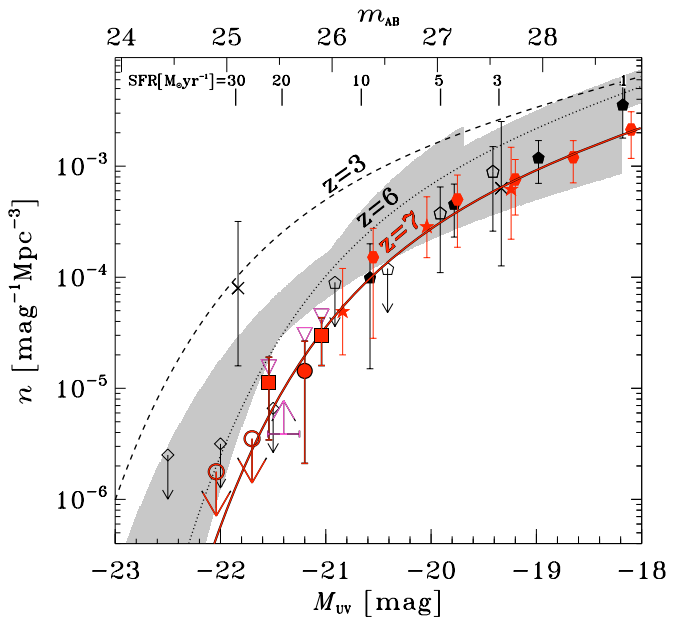

Figure 7. UV luminosity function (LF) of z-dropout galaxies, together with those at lower redshifts. Two red filled squares and one red filled circle present UV LF of our z-dropout galaxies in SDF and GOODS-N, respectively. Two red arrows with open circles indicate upper limits of z-dropout galaxies estimated from our GOODS-N data (right) and the combination of our SDF and GOODS-N data (left). Magenta arrow displays the lower limit estimated from our spectroscopically identified z-dropout galaxy. Magenta inverse-triangles represent the maximal LF, i.e., the secure upper limits of our LF estimates that include no correction for contamination. Recent measurements and upper limits including those from *HST*/WFC3 studies are also plotted with red star marks (Bouwens et al. 2008), hexagons (McLure et al. 2009b), black filled pentagons (Oesch et al. 2009b), open pentagons (Oesch et al. 2009a), open diamonds (Mannucci et al. 2007), and crosses (Richard et al. 2006). Although previous studies define $M_{\rm UV}$ at the rest frame ≃1300−2000 Å, a k-correction between ≃1400 Å and 2000 Å is as small as ∼0.07 (Oesch et al. 2009a). Red solid line plots our best-fit Schechter function of z-dropout galaxies at $z = 7$. Dotted line is UV LF at $z \sim 6$ (Bouwens et al. 2008). Gray shade denotes UV LF from the other various studies (see Figure 22 of Ouchi et al. 2008) including Bunker et al. (2004), Yan & Windhorst (2004), Malhotra et al. (2005), and Bouwens et al. (2006). Dashed line is UV LF at $z \sim 3$ (Steidel et al. 1999). Ticks on the upper horizontal axis show observed broadband magnitudes of objects at $z = 7$. At around the top of this plot, we also tick the corresponding star formation rates estimated from Equation (3) with no dust extinction correction.

[17] We cannot include the recent results of Bunker et al. (2009), Castellano et al. (2009), and Hickey et al. (2009), because their UV LF measurements are not apparently presented.

Table 4
UV Luminosity Function at $z = 7$

ϕ^* (10^{-3}Mpc^{-3})	$M^*_{\rm UV}$ (mag)	α	Mag. Range (mag)	$n^{\rm obs}$ (10^{-3}Mpc^{-3})	$\rho^{\rm obs}_{\rm UV}$ (10^{25}erg s^{-1} Hz^{-1}Mpc^{-3})	$\rho^{\rm upper}_{\rm UV}$ (10^{25}erg s^{-1} Hz^{-1}Mpc^{-3})
(1)	(2)	(3)	(4)	(5)	(6)	(7)
$0.69^{+2.62}_{-0.55}$	-20.10 ± 0.76	-1.72 ± 0.65	$-22.3 < M < -18.0$	$2.2^{+2.3}_{-1.3}$	$4.0^{+6.2}_{-2.6}$	$10.6^{+10.8}_{-5.3}$

Notes. Columns 1–3: Best-fit Schechter parameters. The values of ϕ^* and $M^*_{\rm UV}$ are given in units of 10^{-3}Mpc^{-3} and AB magnitude, respectively. The reduced χ^2 of the fitting is 0.13. Column 4: Magnitude range of UV LFs that are used for the fitting. Columns 5–6: Number density (in 10^{-3} Mpc^{-3}) and UV luminosity density (in 10^{25}erg s^{-1} Hz^{-1} Mpc^{-3}) calculated with the best-fit Schechter parameters down to the limit of UV magnitude, $M_{\rm UV} \leqslant -18$, defined by the *HST*/WFC3 studies. Column 7: The upper limit UV luminosity density which is the integral of the best-fit Schechter function down to $M_{\rm UV} = \infty$.

given set of Schechter parameters.[18] We summarize the best-fit Schechter parameters in Table 4, and plot the best-fit function in Figure 7 with the red line. Although the constraints on α are weak, a steep slope of α is suggestive, which is similar to that at $z \lesssim 6$ (Bouwens et al. 2008; McLure et al. 2009a).

Since our survey results are based on two fields, SDF and GOODS-N, which are well separated on the sky, we can estimate the effect of the cosmic variance on the number densities of z-dropout galaxies. First, the numbers (+Poisson errors) of z-dropout galaxies in samples of SDF and GOODS-N are (2 ± 1.4, 1 ± 1.0) at $y < 25.5$, (4 ± 2.0, 3 ± 1.7) at $y < 25.7$, and (8 ± 2.8, 7 ± 2.6) at $y < 25.9$.[19] Since the survey areas of SDF and GOODS-N are comparable ($\simeq$0.2 deg^2; Section 2.1), the number counts in these two fields are comparable within the errors. Second, we compare the LF measurements of SDF and GOODS-N in Figure 7, and find that the cosmic variance is smaller than a factor of $\sim$2 in number density for the survey areas of 0.2 deg^2. We estimate the expected cosmic variance with the analytic cold dark matter (CDM) model of Sheth & Tormen (1999) from the number density of our z-dropout galaxies down to our magnitude limit ($0.9^{+2.2}_{-0.6} \times 10^{-5}$ Mpc^{-3} at $M_{\rm UV} < 21$), assuming one-to-one correspondence between galaxies and dark halos. The corresponding clustering bias is $b = 7.6$–9.6, and the cosmic variance is 22%–28% for an area of 0.2 deg^2 at $z = 6.5$–7.1. We check our calculations with the Cosmic Variance Calculator[20] (Trenti & Stiavelli 2008), and find that this calculator returns a very comparable number of $\simeq$30% for the cosmic variance after subtraction of Poisson error term. We obtain even a smaller cosmic variance of $\simeq$9%–12% with the CDM model of Sheth & Tormen (1999), if we do not assume the one-to-one correspondence, but adopt clustering bias of galaxies measured at a slightly lower redshift of $z \sim 6$ ($b \simeq$ 3–4; Ouchi et al. 2005; Overzier et al. 2006). Thus, the prediction of CDM model is consistent with our observational constraints of the cosmic variance, $\lesssim$2, in the two areas of 0.2 deg^2.

Figure 8 shows the error ellipses of our Schechter parameters, M^* and ϕ^*, for $\alpha = -1.72$ at the 1σ and 2σ confidence levels. We also present those of LFs at $z = 6$ and 5 (Bouwens et al. 2008; McLure et al. 2009a) and $z = 4$ (Bouwens et al. 2008). Note that all of these Schechter fits are based on $\alpha \simeq -1.7$ ($\alpha = [-1.66] - [-1.74]$ for Bouwens et al. 2008 and $\alpha = [-1.66] - [-1.71]$ for McLure et al. 2009a), and that Figure 8 exclusively compares two parameters of M^* and ϕ^*. Our measurements (red contours in Figure 8) indicate that the Schechter parameters of $z = 7$ LF differ from those of $z \leqslant 6$ LFs significantly, and that LF decreases from $z = 6$ to 7 at more than the 2σ (i.e., 95%) level. Moreover, our constraints of $z = 7$ Schechter parameters are consistent with those of Bouwens et al. (2008; dotted lines in Figure 8), but are stronger than those, which allow us to rule out no evolution at the $> 95\%$ level. Although the errors of our measurements are too large to distinguish between luminosity (L^*) and number (ϕ^*) evolutions, Figure 8 implies that a decrease in L^* would be the dominant factor of the LF evolution from $z =$ 5–6 to 7.

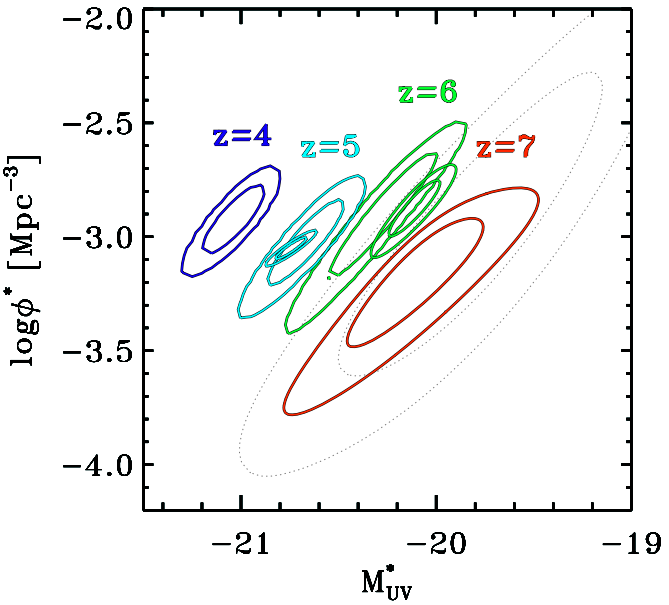

Figure 8. Error ellipses of Schechter parameters, M^* and ϕ^*, at the 1σ and 2σ confidence levels. Red lines represent our results of z-dropout galaxies at $z = 7$. Blue, cyan, and green contours denote error ellipses for galaxies at $z = 4$, 5, and 6 obtained by Bouwens et al. (2008; large contours) and McLure et al. (2009a; small contours only for $z = 5$ and 6). The dotted contours are error ellipses of $z = 7$ galaxies estimated by Bouwens et al. (2008). All of these Schechter fits are based on $\alpha \simeq -1.7$. Our measurements of the red contours indicate that the Schechter parameters of $z = 7$ LF differ from those of $z \leqslant 6$ LFs at the $> 2\sigma$ (i.e., $> 95\%$) level.

4.5. UV Luminosity Density

We calculate UV luminosity densities at $z = 7$ from our UV LF with the best-fit Schechter parameters given in Section 4.4. First, we integrate the LF down to the magnitude of the faintest observed z-dropout galaxies of the *HST*/WFC3 studies, which was used for our Schechter parameter fitting (i.e., down to $M_{\rm UV} = -18$ or $\simeq 0.1L^*$), and obtain the observed UV

[18] To avoid using the dependent measurements from the same *HST* data, we exclude the results of Oesch et al. (2009a, 2009b) in the fitting. The inclusion of Oesch et al. (2009a, 2009b) data does not change our conclusions but with artificially small errors.

[19] Seven (= 15–8) candidates of SDF fall in a narrow magnitude window of $y = 25.9$–26.1, because the test in Section 4.2 indicates that our samples include 0–1 spurious sources. Thus, the moderately large number of faint candidates in SDF is not due to spurious sources but a steep slope of number count for z-dropout galaxies at this magnitude regime.

[20] http://solo.colorado.edu/~trenti/CosmicVariance.html

luminosity density, $\rho_{\rm UV}^{\rm obs}$. Because a total UV luminosity density has to be larger than $\rho_{\rm UV}^{\rm obs}$ by the amount of the contribution from galaxies fainter than the limiting magnitude, $\rho_{\rm UV}^{\rm obs}$ corresponds to the lower limit of the UV luminosity density. We extrapolate our LF down to $L = 0$ to estimate the contribution from such faint galaxies, and obtain the UV luminosity density, $\rho_{\rm UV}^{\rm upper}$. Since there exist no galaxies with $L \sim 0$, this UV luminosity density with the LF extrapolation, $\rho_{\rm UV}^{\rm upper}$, corresponds to the upper limit of UV luminosity density. We estimate $\rho_{\rm UV}^{\rm obs} = 4.0^{+6.2}_{-2.6} \times 10^{25}$ erg s^{-1} Hz^{-1}Mpc^{-3} and $\rho_{\rm UV}^{\rm upper} = 1.1^{+1.1}_{-0.5} \times 10^{26}$ erg s^{-1} Hz^{-1}Mpc^{-3}. Both $\rho_{\rm UV}^{\rm obs}$ and $\rho_{\rm UV}^{\rm upper}$ are summarized in Table 4. We discuss evolution of cosmic star formation rate density (SFRD; Section 5.1) and reionization of the universe (Section 5.2) using these UV luminosity densities. For the upper limit value, there are uncertainties in the faint-end slope of the LF, $\alpha = -1.72$, which we have weakly constrained. If we assume the best-fit Schechter parameters but with a steep slope of $\alpha = -1.86$, $\rho_{\rm UV}^{\rm upper}$ would increase only by a factor of 2, which just corresponds to the 1σ-upper error value (2.2×10^{26} erg s^{-1} Hz^{-1}Mpc^{-3}) of our $\rho_{\rm UV}^{\rm upper}$. On the other hand, a very steep slope of $\alpha = -1.90$ could push up $\rho_{\rm UV}^{\rm upper}$ by a factor of 3, and an extreme value of $\alpha = -1.97$ may boost $\rho_{\rm UV}^{\rm upper}$ by a factor of 10. However, Bouwens et al. (2008) and McLure et al. (2009a) have reported α measurements similar to ours but with a small uncertainty, $\alpha = -1.74 \pm 0.16$ and $\alpha = -1.71 \pm 0.11$, respectively, for galaxies at a slightly lower redshift of $z = 6$. Since it is unlikely that the faint-end slope evolves largely between $z = 6$ and 7, $\rho_{\rm UV}^{\rm upper}$ would not be well beyond its 1σ-upper error value in the reasonable range of α.

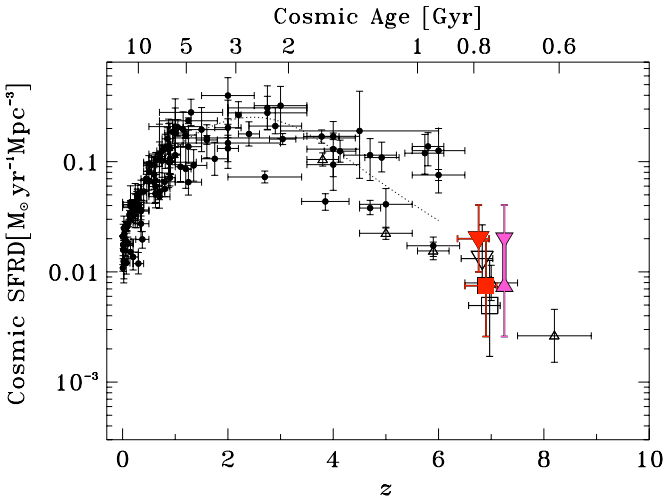

Figure 9. Cosmic star formation rate density (SFRD) as a function of redshift. Red square and inverse-triangle represent the extinction corrected SFRDs integrated down to $L \simeq 0.1L^*$ (SFRD$_{\rm corr}^{\rm obs}$), and to $L = 0$ (SFRD$_{\rm corr}^{\rm upper}$), respectively. Open square and inverse-triangle are the same, but with no extinction correction, i.e., SFRD$^{\rm obs}$ and SFRD$^{\rm upper}$. Magenta line with triangles give the allowed SFRDs at $z = 7$, which are defined by SFRD$^{\rm obs}$ and SFRD$_{\rm corr}^{\rm upper}$ with associated errors. We shift the magenta line with the triangles along the abscissa for the presentation purpose. Filled circles indicate total SFRDs at $z \lesssim 6$ that are compiled by Hopkins & Beacom (2006). Dotted line denotes the best-fit function to the SFRD measurements at $z = 0$–6 with the Cole et al. (2001) formalism (Hopkins & Beacom 2006). Open triangles show SFRD measurements down to $0.06L^*(z = 3)$ with extinction correction, which are recently reported by Bouwens et al. (2009b). Because their $z = 7$ measurement is very close to our results, their triangle symbol at $z = 7$ is hidden behind the red filled square.

5. DISCUSSION

5.1. Cosmic Star Formation History

We calculate cosmic SFRDs from the UV luminosity densities, $\rho_{\rm UV}^{\rm obs}$ and $\rho_{\rm UV}^{\rm upper}$. We use the relation between UV luminosity and star formation rate (SFR) given by Madau et al. (1998):

$$\mathrm{SFR}(M_\odot\ \mathrm{yr}^{-1}) = L_{\rm UV}(\mathrm{erg\ s^{-1}Hz^{-1}})/(8 \times 10^{27}), \quad (3)$$

where $L_{\rm UV}$ is UV luminosity measured at 1500 Å. This relation assumes that galaxies have the Salpeter initial mass function (IMF) with solar metallicity. We obtain SFRD$^{\rm obs} = 4.95^{+7.75}_{-3.24} \times 10^{-3}\ M_\odot$ yr^{-1} Mpc^{-3} and SFRD$^{\rm upper} = 1.32^{+1.35}_{-0.66} \times 10^{-2}\ M_\odot$ yr^{-1} Mpc^{-3} from $\rho_{\rm UV}^{\rm obs}$ and $\rho_{\rm UV}^{\rm upper}$, respectively.

We apply extinction correction to the SFRDs, assuming the empirical relation between the UV slope, β, and extinction, A_{1600}, for starburst galaxies,

$$A_{1600} = 4.43 + 1.99\beta \quad (4)$$

(Meurer et al. 1999). Following the observational results of $z \sim 6$ dropout galaxies (Stanway et al. 2005; Yan et al. 2005; Bouwens et al. 2006, 2007, 2009c), we use $\beta = -2$ for our z-dropout galaxies. We estimate the extinction-corrected SFRDs to be SFRD$_{\rm corr}^{\rm obs} = 7.49^{+11.7}_{-4.90} \times 10^{-3}\ M_\odot$ yr^{-1} Mpc^{-3} and SFRD$_{\rm corr}^{\rm upper} = 2.00^{+2.04}_{-1.00} \times 10^{-2}\ M_\odot$ yr^{-1} Mpc^{-3}. Since SFRD$_{\rm corr}^{\rm upper}$ is the SFRD with dust correction and extrapolation of the LF down to $L = 0$, SFRD$_{\rm corr}^{\rm upper}$ is an upper limit of our SFRD measurements. On the other hand, SFRD$^{\rm obs}$ is the SFRD estimated with neither dust extinction correction nor LF extrapolation. Thus, SFRD$^{\rm obs}$ is regarded as a conservative lower limit.

Figure 9 plots the cosmic SFRDs from our measurements (squares and inverse-triangles) as well as our upper and lower limits including the 1σ errors (magenta line). Figure 9 also displays the cosmic SFRDs obtained from previous studies with the assumption of Salpeter IMF. At $z \simeq 0$–6, we show the cosmic SFRD measurements compiled by Hopkins & Beacom (2006). The compilation of Hopkins & Beacom (2006) covers most of SFRD measurements made, to date, in various wavelength including Hα (Glazebrook et al. 1999; Tresse et al. 2002; Hanish et al. 2006), mid-infrared (Flores et al. 1999; Pérez-González et al. 2005), submm (Barger et al. 2000; Hughes et al. 1998), radio (Condon et al. 2002; Serjeant et al. 2002), and X-ray (Georgakakis et al. 2003). It also includes results of Giavalisco et al. (2004b), Bunker et al. (2004), and Ouchi et al. (2004) for $z > 4$ SFRDs estimated from UV luminosities. Figure 9 presents the best-fit function to the $z \lesssim 6$ SFRD measurements with the Cole et al. (2001) formalism (Hopkins & Beacom 2006). We also plot SFRDs at high redshifts recently reported by Bouwens et al. (2008). The SFRDs of Bouwens et al. (2008) are applied for extinction correction, but integrated down to only $0.2L^*(z = 3)$. Their measurements are interpreted as lower limits of total SFRDs that are counterparts of our SFRD$_{\rm corr}^{\rm obs}$ measurement. Our measurement is consistent with that of Bouwens et al. (2008). In Figure 9, comparing the Hopkins & Beacom's (2006) best-fit model function (dotted line) with our constraints of upper and lower limits (the magenta line with the error bar), we find that the cosmic SFRD drops from the peak at $z = 2$–3 to $z = 7$ roughly by a factor of $\sim$10 (at least by a factor of $\gtrsim$6), but that the drop is not as large as a factor of $\sim$100. Figure 9 indicates that the cosmic SFRD declines even from $z = 6$ to 7, which is originated from the decrease of UV LF from $z = 6$ to 7. Note that this decline of SFRD could be weaker, if there exist

a large population of very faint galaxies, such as suggested by Stark et al. (2007) for $z = 9$–10 galaxies, that the present blank field surveys cannot identify. However, the decreasing tendency of SFRD from $z = 2$–3 to 7 cannot be rejected, if the faint-end LF has a reasonable slope, $\alpha \gtrsim -1.97$, that changes $\rho_{\rm UV}^{\rm upper}$, i.e., $\mathrm{SFRD}_{\rm corr}^{\rm upper}$ by a factor of $\lesssim$10 (see Section 4.5). Because this suppression of SFRD toward high redshifts follows the evolutionary tendency of dark halo mass function such as Sheth & Tormen (1999), this would suggest that we would be witnessing the early phase of galaxy formation history at $z = 7$.

5.2. Ionization Photon Budget Near the Reionization Epoch

We evaluate emission rate of hydrogen ionizing photon per comoving Mpc^3, $\dot{N}_{\rm ion}$, and discuss ionizing photon budget, i.e., whether the photon production rate of galaxies is larger than the recombination rate of hydrogen IGM. We calculate $\dot{N}_{\rm ion}$ for galaxies with

$$\dot{N}_{\rm ion}(\mathrm{s^{-1}\ Mpc^{-3}}) = 10^{49.7}\left(\frac{\epsilon^{\rm g}}{10^{25}}\right)\left(\frac{\alpha_{\rm s}}{3}\right)^{-1}\left(\frac{f_{\rm esc}}{0.1}\right), \quad (5)$$

where $\epsilon^{\rm g}$ is the ionizing emission density at the Lyman limit in units of erg s^{-1}Hz^{-1}Mpc^{-3}, $\alpha_{\rm s}$ is the spectral index of ionizing emission, and $f_{\rm esc}$ is the escape fraction of ionizing photons (Bolton & Haehnelt 2007). We adopt $\epsilon^{\rm g} = \rho_{\rm UV}/6$ for the spectral break at the Lyman limit, where $\rho_{\rm UV}$ is the UV luminosity density at ~1500 Å (Madau et al. 1999), and assume $\alpha_{\rm s} = 3$ that corresponds to a model spectrum of Leitherer et al. (1999) with continuous star formation history, Salpeter IMF, and a metallicity of $Z = 0.2Z_\odot$ (Bolton & Haehnelt 2007). We apply three $f_{\rm esc}$values; $f_{\rm esc} \simeq 0.2$ suggested by the recent numerical simulations of Yajima et al. (2009), $f_{\rm esc} \simeq 0.05$ found in LBGs at $z \sim 3$ (Shapley et al. 2006; see also Iwata et al.'s 2009 subsequent studies), and $f_{\rm esc} = 1.0$ for the maximum escape fraction. Note that $f_{\rm esc} \simeq 0.05$ is also suggested for $z > 4$ galaxies in the semi-analytical model of Wyithe et al. (2009). Figure 10 presents two $\dot{N}_{\rm ion}$ values at $z = 7$ estimated from our $\rho_{\rm UV}^{\rm obs}$ and $\rho_{\rm UV}^{\rm upper}$ with $f_{\rm esc} = 0.2$. We regard these two $\dot{N}_{\rm ion}$ as the lower and upper limits (see Section 4.5). To evaluate the impacts of escape fraction determination, we plot three magenta lines showing the lower and upper limits of $\dot{N}_{\rm ion}$ with the three different escape fractions, $f_{\rm esc} = 0.2$, 0.05, and 1.0. We calculate $\dot{N}_{\rm ion}$ at $z = 4$–6 from the best-fit Schechter parameters of UV LFs obtained by Yoshida et al. (2006), Bouwens et al. (2008), and McLure et al. (2009a). Evaluating upper and lower limits of $\dot{N}_{\rm ion}$ at $z = 4$–6, we integrate UV LFs down to $L = 0$ for the upper limits and down to the observed magnitudes of $M_{\rm UV} \simeq -18$ ($z = 6$), $M_{\rm UV} \simeq -17$ ($z = 5$), and $M_{\rm UV} \simeq -16$ ($z = 4$) for the lower limits of Bouwens et al. (2008) and McLure et al. (2009a).[21] Similarly, we integrate UV LFs down to $M_{\rm UV} = -20.3$ and -19.2 for the lower limits of Yoshida et al. (2006) at $z = 5$ and 4, respectively. These UV luminosity densities are used to estimate $\dot{N}_{\rm ion}$ with Equation (5) and $f_{\rm esc} = 0.2$. Then we add ionizing photons from AGN given by Bolton & Haehnelt (2007), and plot them in Figure 10. We find that $\dot{N}_{\rm ion}$ decreases monotonically from $z = 4$ to 7.

Figure 10 also shows $\dot{N}_{\rm ion}$ that is required to balance recombination of hydrogen IGM based on the model of Madau et al. (1999),

$$\dot{N}_{\rm ion}(\mathrm{s^{-1}\ Mpc^{-3}}) = 10^{47.4} C_{\rm H\,II}(1+z)^3 \quad (6)$$

[21] The measurements of McLure et al. (2009a) include only those at $z = 6$ and 5.

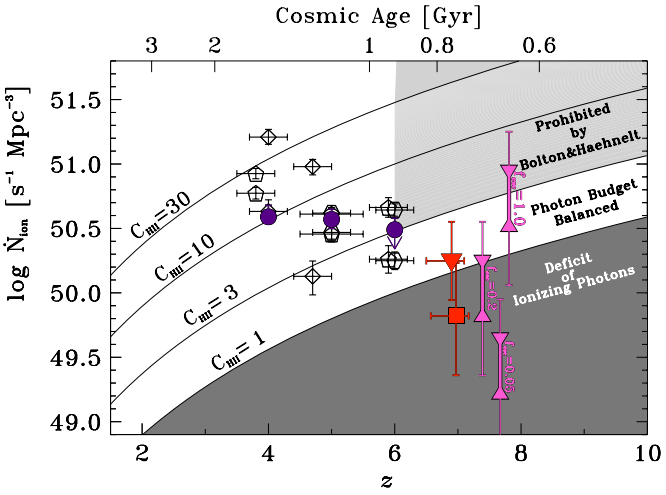

Figure 10. Emission rate of ionizing photon per comoving Mpc^3, $\dot{N}_{\rm ion}$, as a function of redshift. We assume $f_{\rm esc} = 0.2$, if not otherwise specified. Square and triangle present the lower and upper limits of $\dot{N}_{\rm ion}$ at $z \simeq 7$ estimated from $\rho_{\rm UV}^{\rm obs}$ and $\rho_{\rm UV}^{\rm upper}$, respectively. Three thick magenta lines with triangle/inverse-triangle represent the allowed $\dot{N}_{\rm ion}$ ranges at $z = 7$ for $f_{\rm esc} = 0.2$, 0.05, and 1.0 from left to right. These ranges are defined by the lower and upper limits of $\dot{N}_{\rm ion}$. Thin magenta lines denote the associated 1σ errors corresponding to 1σ errors of the upper and lower limit estimates. For the presentation purpose, we shift the red square and the magenta lines along the abscissa. The exact redshift is the same as the one of red triangle. Solid lines plot the model predictions of $\dot{N}_{\rm ion}$ that is required for maintaining hydrogen ionization in IGM (Madau et al. 1999) with clumping factors of $C_{\rm H\,II} = 1$, 3, 10, and 30, from bottom to top. Dark gray area indicates that even the homogeneous universe ($C_{\rm H\,II} = 1$) lacks ionizing photons to maintain hydrogen ionization of IGM in the model of Madau et al. (1999). The photoionization rates inferred from the Lyα forest are shown with purple circles (Bolton & Haehnelt 2007). Light gray shade displays constraints from Bolton & Haehnelt (2007), who find that the clumping factor is $C_{\rm H\,II} \lesssim 3$ at $z \sim 6$ (and at $z \gtrsim 6$ in the hierarchical universe). Diamonds and pentagons are $\dot{N}_{\rm ion}$ at $z = 4$–6 produced by both AGN and galaxies that are calculated from AGN LFs (Bolton & Haehnelt 2007) and galaxy LFs given by Yoshida et al. (2006) and Bouwens et al. (2008), respectively. Upper and lower sequences of diamonds/pentagons present the upper and lower limits of $\dot{N}_{\rm ion}$ calculated from their LFs down to the observation limiting luminosities and $L = 0$, respectively, which are counterparts of our $\rho_{\rm UV}^{\rm obs}$ and $\rho_{\rm UV}^{\rm upper}$ measurements. Although our $\dot{N}_{\rm ion}$ at $z = 7$ includes no AGN contribution due to no AGN LF measurements at $z = 7$, the contribution of AGN is probably smaller than $\lesssim$0.08 dex at $\log \dot{N}_{\rm ion} \simeq 50$ (see the text).

with clumping factors of $C_{\rm H\,II} = 1$, 3, 10, and 30. Note that $C_{\rm H\,II} = 1$ corresponds to the homogeneous universe, and that the universe at $z \sim 7$ should have $C_{\rm H\,II} > 1$ due to the hierarchical structure formation. If the photon production rates of objects fall below the model of $C_{\rm H\,II} = 1$, hydrogen IGM cannot maintain the ionized state for any clumping factors taken at the redshift. On the other hand, the photoionization rates inferred from the Lyα forest indicate that clumping factor is as small as $C_{\rm H\,II} \lesssim 3$ at $z \sim 6$ (Bolton & Haehnelt 2007; the purple circles in Figure 10). Since $C_{\rm H\,II}$ should monotonically decrease toward high redshifts in the hierarchical universe, the models with $C_{\rm H\,II} \lesssim 3$ can be applied to the universe at $z \gtrsim 6$. If $\dot{N}_{\rm ion}$ of objects falls in or beyond the model of $1 < C_{\rm H\,II} \lesssim 3$ at $z \gtrsim 6$, the ionizing photon production rate is high enough to maintain the ionized IGM.

Figure 10 presents that, in the cases of $f_{\rm esc} = 0.2$ and $f_{\rm esc} = 1.0$, $\dot{N}_{\rm ion}$ values of $z = 7$ galaxies are comparable with those predicted by the models of $1 < C_{\rm H\,II} \lesssim 3$. We do not include the AGN contribution of $\dot{N}_{\rm ion}$ to our estimate at $z = 7$, because no AGN UV LF data are available at this redshift. However, AGN contribution of ionizing photon production is only $\log \dot{N}_{\rm ion} \simeq 49.3$ at $z = 6$ (Bolton & Haehnelt 2007). Because the comoving density of luminous QSOs at $z \sim 6$

is 30 times smaller than that at $z \sim 3$ (Fan et al. 2004), AGN LF probably continues decreasing toward $z \sim 7$. Even if we assume no evolution of AGN LF from $z = 6$ to 7, the AGN contribution is negligible; only pushing 0.08 dex at $\log \dot{N}_{\rm ion} \simeq 50$ in Figure 10.

Our results indicate that the ionizing photon budget just balances at $z = 7$ for $f_{\rm esc} \gtrsim 0.2$. On the other hand, $\dot{N}_{\rm ion}$ of $z = 7$ galaxies with $f_{\rm esc} = 0.05$ is a factor of 3 below the model of $C_{\rm H\,II} = 1$, which has the $\simeq$95% (2σ) confidence level. Note that $f_{\rm esc} \simeq 0.05$ is the measured escape fraction at $z \sim 3$ (Shapley et al. 2006). Moreover, all of the other parameters for our $\dot{N}_{\rm ion}$ estimates, i.e., the spectral index and break, are plausible ones for low-z star-forming galaxies. Thus, there are two scenarios. (1) If no properties of star-forming galaxies at $z = 7$ are different from those at low redshifts, the universe could not be totally ionized by only galaxies (and AGN) at $z = 7$ at the $\simeq$95% confidence level. (2) If the properties of star-forming galaxies evolve from low redshifts, e.g., larger $f_{\rm esc}$ ($f_{\rm esc} \gtrsim 0.2$), lower metallicity, flatter IMF, and/or less dust extinction, the universe at $z = 7$ is ionized and close to being in balance between the rates of ionizing photon production and recombination of hydrogen IGM. If the scenario (1) is true, the hydrogen IGM would experience a deficit of ionizing photon at $z = 7$. This implies that the universe may not complete the reionization by $z = 7$. In this case, the universe would start reionization right after $z = 7$ and almost complete it by $z \sim 6$ (Fan et al. 2006). However, the polarization data of WMAP5 place the constraints that instantaneous reionization below $z = 8.2$ ($= 6.7$) is rejected at the 2σ (3σ) level (Dunkley et al. 2009). It is unlikely that reionization of the universe is completed at the late epoch of $z \sim 6$–7 almost instantaneously. Alternatively, the scenario of (1) indicates that not galaxies and AGN but some exotic populations or physical phenomena might play an important role in cosmic reionization. Although several candidates of the exotic ionizing sources are suggested, such as dark matter annihilation and primordial black holes (e.g., Ricotti & Ostriker 2004; Ricotti et al. 2008), no observational evidence have been obtained. It is more likely that the scenario (2) is correct, and that the escape fraction, metallicity, IMF, and dust extinction are larger, lower, flatter, and/or smaller, respectively. In fact, Inoue et al. (2006) claim that $f_{\rm esc}$ increases toward high redshifts at $0 < z < 6$ via their model calculations. The numerical simulations of Razoumov & Sommer-Larsen (2009) also suggest the similar evolution of $f_{\rm esc}$, which reaches 0.8 at $z = 10$, and that the angular averaged escape fraction of $f_{\rm esc} = 0.3$–0.6 at $z \sim 7$ for galaxies similar to ours (SFR$\simeq$1–10 $M_\odot$). Metallicity of galaxies also have an impact on the production of ionizing photons. Stiavelli et al. (2004) claim that the ionizing efficiency of a stellar population increases by a factor of 3 for Salpeter IMF and a factor of 10 for a top-heavy IMF as the metallicity decreases from $Z = Z_\odot$ to $Z = 0$ (see also Schaerer 2003).[22] Moreover, dust absorption may be important in determination of escape fraction, as demonstrated by the simulations of Laursen et al. (2009). Because Lyα emissivity would be higher at $z \sim 6$ than low-z as suggested by LAE studies (e.g., Ouchi et al. 2008), a flatter IMF as well as lower metallicity and/or less dust extinction toward high-z may be plausible. It should be noted that, even in the scenario (2), our observational constraints are close to being in balance between ionizing photon production and recombination rates at $z \sim 7$. In other words, we might be witnessing the final stage of reionization with the closely balanced photon budget. It would provide signatures of the neutral fraction evolution that are claimed by Iye et al. (2006) and Ota et al. (2008), who find significantly less number of LAEs at $z \sim 7$ than $z \sim 6$. Moreover, the scenario of (2) is very consistent with the extended ($z \sim 6$–11) reionization picture suggested by Dunkley et al. (2009). Note that these arguments assume that there is no emergence of a large population of very faint galaxies at $z = 7$ beyond the Schechter function, such as claimed by Stark et al. (2007) for the earlier epoch of $z = 9$–10. On the other hand, Santos et al. (2004) have found that star formation activities of low-mass galaxies are suppressed at $z \simeq 5$ via their Keck gravitational lensing survey. Systematic lensing surveys for $z = 7$ galaxies would be needed to correctly understand the contribution from these very faint galaxies. Although there remain the arguments of the very faint galaxy population, the $\dot{N}_{\rm ion}$ of $z = 7$ galaxies with $f_{\rm esc} = 0.05$ still falls below the model of $C_{\rm H\,II} = 1$ with a very steep faint-end slope down to $\alpha \simeq -1.90$ that would boosts $\rho_{\rm UV}^{\rm upper}$, i.e., the upper limit of $\dot{N}_{\rm ion}$ by a factor of $\simeq$3 (Section 4.5).

5.3. Distribution of Dropouts: Indication of Ionized Bubble?

Figure 11 presents the sky distribution of our z-dropout galaxies in SDF and GOODS-N. Although the numbers of galaxies in each field are small, they appear to be clustered on the sky. The distribution in SDF shows possible three filamentary structures crossing at around the center of the field; from top to the center, the center to bottom right, and the center to bottom left. The possible filaments would extend up to $\sim$60 Mpc. Our dropout galaxies in GOODS-N are located mostly at the center right and top left. These sky distributions imply that our $z = 7$ galaxies with a bright UV luminosity ($M_{\rm UV} \sim -21$; ${\rm SFR}_{\rm nodust} = 10$–30) would be strongly clustered, which are similar to those at $z \sim 6$ (Ouchi et al. 2005; Overzier et al. 2006; Lee et al. 2009). In Figure 11, we mark the positions of the UV brightest galaxies with $y < 25.6$ among our galaxies at $z = 7$. We find that these brightest galaxies are located at the high density regions of z-dropout galaxies both in SDF and GOODS-N. In the SDF panel of Figure 11, we also mark the Lyα emitting dropout galaxy, SDF-63544, at $z_{\rm spec} = 6.96$ confirmed by spectroscopy (Iye et al. 2006). Interestingly, this Lyα emitting dropout galaxy sits at the center of the four UV brightest dropout galaxies whose distribution extends by $\sim$30 Mpc in projection (Figure 11). Because Ota et al. (2008) did not confirm the other LAE candidate found by their narrowband survey of $z = 7$ even with their deep spectroscopic data, this SDF-63544 may be only one with an observable Lyα emission line at $z = 7$ in the SDF. It would be possible that an overdense region of the four UV brightest dropouts would make a well-established ionized bubble of IGM in the cosmic volume with a size of $\gtrsim$30 Mpc, and that the ionized bubble may allow SDF-63544 to transmit Lyα to observers with no strong Lyα damping absorption given by neutral hydrogen of IGM. To evaluate how much Lyα flux is absorbed by IGM, we estimate a Lyα equivalent width of the Lyα emitting dropout galaxy from the UV continuum magnitude (-21.40 ± 0.31) and Lyα flux (2×10^{-17} erg s^{-1} cm^{-2}; see Section 4.4), and obtain the rest-frame equivalent width of ${\rm EW}_0 = 37 \pm 8$ Å. This ${\rm EW}_0$ is about a half of the one for the case B recombination with no absorption of Lyα (68 Å; Nagamine et al. 2008; Ono et al. 2009). We define the escape fraction of Lyα emission,

[22] Since the temperature of IGM increases from 10,000 K (for the solar metallicity) to $\sim$20,000 K (for low metallicity; Osterbrock 1989), the low metallicity in IGM would reduce the recombination rate of IGM with the solar metallicity by a factor of $\sim$2 (Stiavelli et al. 2004).

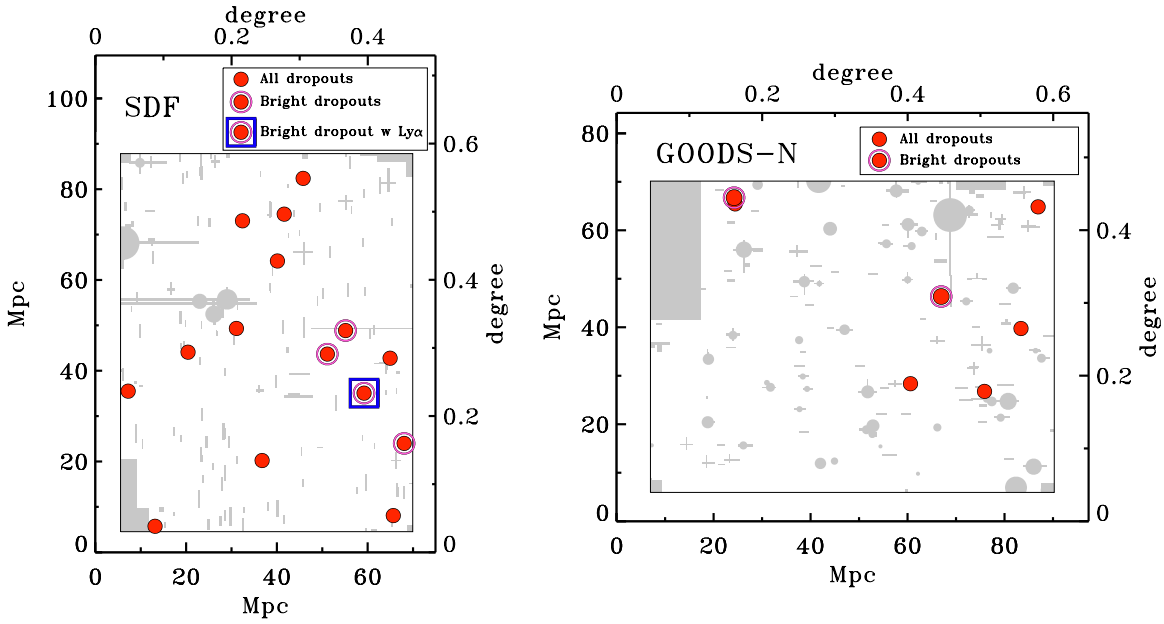

Figure 11. Sky distribution of our $z = 7$ dropout galaxies down to $y = 26.1$ in SDF (left panel) and down to $y = 25.9$ in GOODS-N (right panel). Red circles represent positions of all dropout galaxies, while red circles with a magenta circle denote bright dropouts with $y < 25.6$. Blue square indicates the position of the bright dropout with Lyα emission at $z_{\rm spec} = 6.96$. Gray shades are masked areas where we did not use the data for our analysis. The scales on the maps are marked in both degrees and comoving megaparsecs in projection at $z = 7$. North is up and east is to the left in these images.

$f_{\rm esc}^{\rm Ly\alpha}$, by

$$f_{\rm esc}^{\rm Ly\alpha} = \frac{L_{\rm obs}^{\rm Ly\alpha}}{L_{\rm int}^{\rm Ly\alpha}}, \quad (7)$$

where $L_{\rm obs}^{\rm Ly\alpha}$ and $L_{\rm int}^{\rm Ly\alpha}$ are observed and intrinsic Lyα luminosities, respectively. If we assume the case B recombination, $L_{\rm int}^{\rm Ly\alpha}[{\rm erg\ s^{-1}}] = 1.1 \times 10^{42}\ {\rm SFR}[M_\odot\ {\rm yr^{-1}}]$, and SFR from $M_{\rm UV}$ with no dust extinction correction (Equation (3)),[23] we estimate the Lyα escape fraction of the Lyα emitting dropout to be $f_{\rm esc}^{\rm Ly\alpha} = 0.54 \pm 0.12$. This $f_{\rm esc}^{\rm Ly\alpha}$ would be comparable to the one at $z \sim 6$ with no strong IGM damping wing of Lyα, because the average Lyα escape fraction is $f_{\rm esc}^{\rm Ly\alpha} = 0.52$–$0.54$ at $z \sim 6$ estimated from the Lyα opacities of Fan et al. (2006), Madau (1995), and Meiksin (2006) for the case that IGM absorbs a blue half of symmetric Lyα emission line (see Section 5.1.2 of Ouchi et al. 2008). The inferred $f_{\rm esc}^{\rm Ly\alpha}$ would support the idea that the Lyα emitting dropout galaxy sits inside a well-established ionized bubble with a neutral fraction as low as that at $z \sim 6$.

If this naive physical picture is correct, the size of ionized bubble would be larger than 30 Mpc at $z = 7$. Assuming that this is a lower limit of the characteristic bubble size, we find that the analytic models of Furlanetto et al. (2006) would suggest an upper limit of neutral fraction of $x_{\rm H\,I} \lesssim 20\%$ at $z = 7$. This small upper limit of $x_{\rm H\,I}$ may indicate that the universe is not fully neutral at $z = 7$. The combination of reionization models and LAE LF (+clustering) gives constraints on neutral fraction of $x_{\rm H\,I} \lesssim 50\%$ at $z = 6.5$ (Dijkstra et al. 2007; McQuinn et al. 2007; Iliev et al. 2008) and $x_{\rm H\,I} \lesssim 10\%$–$60\%$ at $z = 7$ (Kobayashi et al. 2007; Ota et al. 2008). Our possible upper limit of $x_{\rm H\,I} \lesssim 20\%$ at $z = 7$ is consistent with those of previous results from the independent observational probes. This implies that there is no strong evidence rejecting the presence of the $\gtrsim$30 Mpc ionized bubble at $z = 7$.

[23] SFR thus obtained is 19.7 $M_\odot\ {\rm yr^{-1}}$ for the Lyα emitting dropout.

6. CONCLUSIONS

We have identified 22 z-dropout galaxy candidates in the 0.4 deg^2 area of SDF and GOODS-N down to $y = 26$ with deep $\simeq$30 hr *Subaru* y-band images and *Subaru* and *HST* legacy imaging data. One out of 22 z-dropout galaxies in the SDF has a spectroscopic redshift of $z = 6.96$ determined from Lyα emission. We have derived the bright-end UV LF of galaxies at $z = 7$. Based on our bright z-dropout galaxies as well as faint z-dropout galaxies obtained by the recent *HST*/WFC3 studies, we have constrained the early stage of galaxy formation and photon budget of cosmic reionization at $z = 7$. We have also discussed the distributions of our z-dropout galaxies. The major results of our study are summarized below.

1. We find that our bright-end UV LF shows a decrease from $z \sim 6$ to 7. This decrease cannot be explained by statistical errors or cosmic variance that is less than a factor of $\lesssim$2 in number density for a 0.2 deg^2 area. The best-fit Schechter parameters of $z = 7$ galaxies are $\phi^* = 0.69^{+2.62}_{-0.55} \times 10^{-3}$ Mpc^{-3}, $M_{\rm UV}^* = -20.10 \pm 0.76$ mag, and $\alpha = -1.72 \pm 0.65$. Our Schechter parameter fit results reject no evolution of UV LF from $z = 6$ to 7 at the $> 95\%$ confidence level. A more dominant decrease of L^* than ϕ^* is preferable from $z = 5$–6 to 7 in the error contours of Schechter parameters.
2. The cosmic SFRD drops from $z = 2$–3 to $z = 7$ by a factor of at least $\gtrsim$6. It is likely that the cosmic SFRD decreases roughly by a factor of $\sim$10, but not larger than $\sim$100. This suppression of cosmic SFRD implies that we would be witnessing the early phase of galaxy formation history.
3. If we assume the properties of low-z star-forming galaxies, including the spectral shape and escape fraction ($f_{\rm esc} \simeq 0.05$), we find that the ionized photon production rate of $z = 7$ galaxies falls below the hydrogen IGM recombination rate predicted by the analytic models of Madau et al. (1999) even in the homogeneous universe ($C_{\rm H\,II} = 1$) at the $\simeq$95% (2σ) confidence level. Although it implies that

the universe cannot be totally ionized by only galaxies at $z = 7$, but we think that properties of galaxies at $z = 7$ are just different from those at low redshifts with, e.g., a larger escape fraction ($f_{\rm esc} \gtrsim 0.2$), a lower metallicity, a flatter IMF, and/or less dust extinction. In either case, our observational constraints imply that the universe at $z \sim 7$ is close to being in balance between rates of ionizing photon production and IGM hydrogen recombination.

4. z-dropout galaxies may be strongly clustered both in SDF and GOODS-N. We find that the distribution of z-dropout galaxies in SDF appears to be a filamentary shape that extends up to 60 Mpc in projection, and that the $z = 6.96$ dropout galaxy with a Lyα line is located at the center of the overdense region consisting of the four UV brightest dropout galaxy candidates. This implies that there may exist a well-established ionized bubble made by the four UV brightest dropout galaxies, and that the ionized bubble might help to transmit the Lyα line in IGM at $z = 7$.

We thank Ross Mclure, Rychard Bouwens, Pascal Oesch, and Andrew Hopkins for providing their data. We are grateful to Rychard Bouwens, Daniel Schaerer, Wei Zheng, Min-Su Shin, and David Sobral for their useful comments. We acknowledge the current and former Subaru Observatory staff, especially Hisanori Furusawa, Akito Tajitsu, Miki Ishii, Michihiro Takami, and Fumiaki Nakata, for their invaluable help that made this challenging and long-standing project possible. M.O. expresses deep gratitude to Shigeru Fukushima who had given M.O. aid and comfort for the past six years beyond this project. M.O. has been supported via Carnegie Fellowship.

Facility: Subaru (Suprime-Cam)

REFERENCES

Barger, A. J., Cowie, L. L., & Richards, E. A. 2000, AJ, 119, 2092
Barger, A. J., Cowie, L. L., & Wang, W.-H. 2008, ApJ, 689, 687
Becker, G. D., Rauch, M., & Sargent, W. L. W. 2007, ApJ, 662, 72
Bertin, E., & Arnouts, S. 1996, A&AS, 117, 393
Bohlin, R. C., Colina, L., & Finley, D. S. 1995, AJ, 110, 1316
Bolton, J. S., & Haehnelt, M. G. 2007, MNRAS, 382, 325
Bouwens, R. J., Illingworth, G. D., Blakeslee, J. P., & Franx, M. 2006, ApJ, 653, 53
Bouwens, R. J., Illingworth, G. D., Franx, M., & Ford, H. 2007, ApJ, 670, 928
Bouwens, R. J., Illingworth, G. D., Franx, M., & Ford, H. 2008, ApJ, 686, 230
Bouwens, R. J., et al. 2009a, ApJ, 690, 1764
Bouwens, R. J., et al. 2009b, arXiv:0909.1803
Bouwens, R. J., et al. 2009c, arXiv:0909.4074
Bradley, L. D., et al. 2008, ApJ, 678, 647
Bruzual, G., & Charlot, S. 2003, MNRAS, 344, 1000
Bunker, A. J., Stanway, E. R., Ellis, R. S., & McMahon, R. G. 2004, MNRAS, 355, 374
Bunker, A., et al. 2009, arXiv:0909.2255
Capak, P., et al. 2004, AJ, 127, 180
Castellano, M., et al. 2009, arXiv:0909.2853
Cimatti, A., et al. 2002, A&A, 381, L68
Cohen, J. G. 2001, AJ, 121, 2895
Cohen, J. G., Hogg, D. W., Blandford, R., Cowie, L. L., Hu, E., Songaila, A., Shopbell, P., & Richberg, K. 2000, ApJ, 538, 29
Cole, S., et al. 2001, MNRAS, 326, 255
Coleman, G. D., Wu, C.-C., & Weedman, D. W. 1980, ApJS, 43, 393
Condon, J. J., Cotton, W. D., & Broderick, J. J. 2002, AJ, 124, 675
Dawson, S., Stern, D., Bunker, A. J., Spinrad, H., & Dey, A. 2001, AJ, 122, 598
Dickinson, M., Giavalisco, M., & The Goods Team 2003, in Proc. ESO, The Mass of Galaxies at Low and High Redshift, ed. R. Bender & A. Renzini (Berlin: Springer), 324
Dijkstra, M., Wyithe, J. S. B., & Haiman, Z. 2007, MNRAS, 379, 253
Dow-Hygelund, C. C., et al. 2007, ApJ, 660, 47
Dunkley, J., et al. 2009, ApJS, 180, 306
Eddington, A. S. 1940, MNRAS, 100, 354
Eyles, L. P., Bunker, A. J., Ellis, R. S., Lacy, M., Stanway, E. R., Stark, D. P., & Chiu, K. 2007, MNRAS, 374, 910
Fan, X., et al. 2004, AJ, 128, 515
Fan, X., et al. 2006, AJ, 132, 117
Flores, H., et al. 1999, ApJ, 517, 148
Furlanetto, S. R., Zaldarriaga, M., & Hernquist, L. 2006, MNRAS, 365, 1012
Georgakakis, A., Hopkins, A. M., Sullivan, M., Afonso, J., Georgantopoulos, I., Mobasher, B., & Cram, L. E. 2003, MNRAS, 345, 939
Giavalisco, M., et al. 2004a, ApJ, 600, L93
Giavalisco, M., et al. 2004b, ApJ, 600, L103
Glazebrook, K., Blake, C., Economou, F., Lilly, S., & Colless, M. 1999, MNRAS, 306, 843
Gunn, J. E., & Stryker, L. L. 1983, ApJS, 52, 121
Hanish, D. J., et al. 2006, ApJ, 649, 150
Hayashi, M., et al. 2009, ApJ, 691, 140
Henry, A. L., Malkan, M. A., Colbert, J. W., Siana, B., Teplitz, H. I., & McCarthy, P. 2008, ApJ, 680, L97
Henry, A. L., Malkan, M. A., Colbert, J. W., Siana, B., Teplitz, H. I., McCarthy, P., & Yan, L. 2007, ApJ, 656, L1
Henry, A. L., et al. 2009, ApJ, 697, 1128
Hickey, S., Bunker, A., Jarvis, M. J., Chiu, K., & Bonfield, D. 2009, arXiv:0909.4205
Hopkins, A. M., & Beacom, J. F. 2006, ApJ, 651, 142
Hughes, D. H., et al. 1998, Nature, 394, 241
Iliev, I. T., Shapiro, P. R., McDonald, P., Mellema, G., & Pen, U.-L. 2008, MNRAS, 391, 63
Inoue, A. K., & Iwata, I. 2008, MNRAS, 387, 1681
Inoue, A. K., Iwata, I., & Deharveng, J.-M. 2006, MNRAS, 371, L1
Iwata, I., et al. 2009, ApJ, 692, 1287
Iye, M., et al. 2006, Nature, 443, 186
Kamata, Y., et al. 2008, Proc. SPIE, 7021, 52
Kashikawa, N., et al. 2003, AJ, 125, 53
Kashikawa, N., et al. 2004, PASJ, 56, 1011
Kashikawa, N., et al. 2006, ApJ, 648, 7
Knapp, G. R., et al. 2004, AJ, 127, 3553
Kobayashi, M. A. R., Totani, T., & Nagashima, M. 2007, ApJ, 670, 919
Laursen, P., Sommer-Larsen, J., & Andersen, A. C. 2009, ApJ, 704, 1640
Lee, K.-S., Giavalisco, M., Conroy, C., Wechsler, R. H., Ferguson, H. C., Somerville, R. S., Dickinson, M. E., & Urry, C. M. 2009, ApJ, 695, 368
Leitherer, C., et al. 1999, ApJS, 123, 3
Lowenthal, J. D., et al. 1997, ApJ, 481, 673
Ly, C., et al. 2009, ApJ, 697, 1410
Madau, P. 1995, ApJ, 441, 18
Madau, P., Haardt, F., & Rees, M. J. 1999, ApJ, 514, 648
Madau, P., Pozzetti, L., & Dickinson, M. 1998, ApJ, 498, 106
Malhotra, S., et al. 2005, ApJ, 626, 666
Mannucci, F., Buttery, H., Maiolino, R., Marconi, A., & Pozzetti, L. 2007, A&A, 461, 423
McLure, R. J., Cirasuolo, M., Dunlop, J. S., Foucaud, S., & Almaini, O. 2009a, MNRAS, 395, 2196
McLure, R. J., Dunlop, J. S., Cirasuolo, M., Koekemoer, A. M., Sabbi, E., Stark, D. P., Targett, T. A., & Ellis, R. S. 2009b, arXiv:0909.2437
McQuinn, M., Hernquist, L., Zaldarriaga, M., & Dutta, S. 2007, MNRAS, 381, 75
Meiksin, A. 2006, MNRAS, 365, 807
Meurer, G. R., Heckman, T. M., & Calzetti, D. 1999, ApJ, 521, 64
Miyazaki, S., et al. 2002, PASJ, 54, 833
Morokuma, T., et al. 2008, ApJ, 676, 163
Nagamine, K., Ouchi, M., Springel, V., & Hernquist, L. 2008, arXiv:0802.0228
Nagao, T., et al. 2007, A&A, 468, 877
Oesch, P. A., et al. 2009a, ApJ, 690, 1350
Oesch, P. A., et al. 2009b, arXiv:0909.1806
Oke, J. B. 1990, AJ, 99, 1621
Ono, Y., et al. 2009, MNRAS, submitted
Osterbrock, D. E. 1989, Astrophysics of Gaseous Nebulae and Active Galactic Nuclei (Mill Valley, CA: Univ. Science Books)
Ota, K., et al. 2008, ApJ, 677, 12
Ouchi, M., et al. 2004, ApJ, 611, 660
Ouchi, M., et al. 2005, ApJ, 620, L1
Ouchi, M., et al. 2008, ApJS, 176, 301
Ouchi, M., et al. 2009, ApJ, 696, 1164
Overzier, R. A., Bouwens, R. J., Illingworth, G. D., & Franx, M. 2006, ApJ, 648, L5
Papovich, C., Dickinson, M., & Ferguson, H. C. 2001, ApJ, 559, 620
Pérez-González, P. G., et al. 2005, ApJ, 630, 82

Phillips, A. C., Guzman, R., Gallego, J., Koo, D. C., Lowenthal, J. D., Vogt, N. P., Faber, S. M., & Illingworth, G. D. 1997, ApJ, 489, 543
Poznanski, D., et al. 2007, MNRAS, 382, 1169
Razoumov, A. O., & Sommer-Larsen, J. 2009, arXiv:0903.2045
Reddy, N. A., Steidel, C. C., Erb, D. K., Shapley, A. E., & Pettini, M. 2006, ApJ, 653, 1004
Richard, J., Pelló, R., Schaerer, D., Le Borgne, J.-F., & Kneib, J.-P. 2006, A&A, 456, 861
Richard, J., Stark, D. P., Ellis, R. S., George, M. R., Egami, E., Kneib, J.-P., & Smith, G. P. 2008, ApJ, 685, 705
Richmond, M. W., Morokuma, T., Doi, M., Komiyama, Y., Yasuda, N., Okamura, S., & Gal-Yam, A. 2009, PASJ, 61, 97
Ricotti, M., & Ostriker, J. P. 2004, MNRAS, 352, 547
Ricotti, M., Ostriker, J. P., & Mack, K. J. 2008, ApJ, 680, 829
Ryan, R. E., Jr., Hathi, N. P., Cohen, S. H., & Windhorst, R. A. 2005, ApJ, 631, L159
Santos, M. R., Ellis, R. S., Kneib, J.-P., Richard, J., & Kuijken, K. 2004, ApJ, 606, 683
Schaerer, D. 2003, A&A, 397, 527
Schaerer, D., & de Barros, S. 2009, A&A, 502, 423
Schlegel, D. J., Finkbeiner, D. P., & Davis, M. 1998, ApJ, 500, 525
Serjeant, S., Gruppioni, C., & Oliver, S. 2002, MNRAS, 330, 621
Shapley, A. E., Steidel, C. C., Pettini, M., & Adelberger, K. L. 2003, ApJ, 588, 65
Shapley, A. E., Steidel, C. C., Pettini, M., Adelberger, K. L., & Erb, D. K. 2006, ApJ, 651, 688
Sheth, R. K., & Tormen, G. 1999, MNRAS, 308, 119
Shimasaku, K., Ouchi, M., Furusawa, H., Yoshida, M., Kashikawa, N., & Okamura, S. 2005, PASJ, 57, 447
Shimasaku, K., et al. 2003, ApJ, 586, L111
Shimasaku, K., et al. 2006, PASJ, 58, 313
Sobral, D., et al. 2009, MNRAS, 398, L68
Stanway, E. R., Bunker, A. J., McMahon, R. G., Ellis, R. S., Treu, T., & McCarthy, P. J. 2004a, ApJ, 607, 704
Stanway, E. R., McMahon, R. G., & Bunker, A. J. 2005, MNRAS, 359, 1184
Stanway, E. R., et al. 2004b, ApJ, 604, L13
Stanway, E. R., et al. 2007, MNRAS, 376, 727
Stark, D. P., Ellis, R. S., Richard, J., Kneib, J.-P., Smith, G. P., & Santos, M. R. 2007, ApJ, 663, 10
Steidel, C. C., Adelberger, K. L., Giavalisco, M., Dickinson, M., & Pettini, M. 1999, ApJ, 519, 1
Steidel, C. C., Adelberger, K. L., Shapley, A. E., Pettini, M., Dickinson, M., & Giavalisco, M. 2003, ApJ, 592, 728
Steidel, C. C., Giavalisco, M., Dickinson, M., & Adelberger, K. L. 1996, AJ, 112, 352
Stiavelli, M., Fall, S. M., & Panagia, N. 2004, ApJ, 610, L1
Trenti, M., & Stiavelli, M. 2008, ApJ, 676, 767
Tresse, L., Maddox, S. J., Le Fèvre, O., & Cuby, J.-G. 2002, MNRAS, 337, 369
Vanzella, E., et al. 2006, A&A, 454, 423
Wirth, G. D., et al. 2004, AJ, 127, 3121
Wyithe, S., Hopkins, A. M., Kistler, M. D., Yuksel, H., & Beacom, J. F. 2009, arXiv:0908.0193
Yagi, M., Kashikawa, N., Sekiguchi, M., Doi, M., Yasuda, N., Shimasaku, K., & Okamura, S. 2002, AJ, 123, 66
Yajima, H., Umemura, M., Mori, M., & Nakamoto, T. 2009, MNRAS, 398, 715
Yan, H., Dickinson, M., Giavalisco, M., Stern, D., Eisenhardt, P. R. M., & Ferguson, H. C. 2006, ApJ, 651, 24
Yan, H., & Windhorst, R. A. 2004, ApJ, 612, L93
Yan, H., et al. 2004, ApJ, 616, 63
Yan, H., et al. 2005, ApJ, 634, 109
Yoshida, M., et al. 2006, ApJ, 653, 988
Zheng, W., et al. 2009, ApJ, 697, 1907